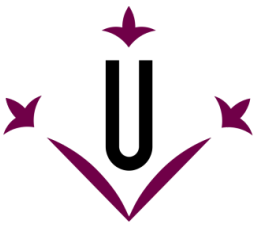

Hydroxytyrosol and its main plasma circulating metabolites attenuate the initial steps of atherosclerosis through inhibition of the MAPK pathway

Authors:

Úrsula Catalán[1], Maria-Carmen López de las Hazas[2], Carmen Piñol[3], Laura Rubió[1, 2 †], Maria-José Motilva[2†], Sara Fernandez-Castillejo[1] and Rosa Solà[1]

[1] Functional Nutrition, Oxidation and Cardiovascular Diseases Group (NFOC-Salut), Hospital Universitari Sant Joan (HUSJR), Institut d'Investigació Sanitaria Pere Virgili (IISPV), Technological Center of Nutrition and Health (CTNS), Faculty of Medicine and Health Sciences, Universitat Rovira i Virgili, Sant Llorenç, 21, 43201, Reus, Spain

[2] Food Technology Department, Universitat de Lleida-AGROTECNIO Center, Alcalde Rovira Roure 191, 25198 Lleida, Spain

[3] Department of Medicine, Facultat de Medicina, University of Lleida, Avda/Alcalde Rovira Roure 80, 25198 Lleida, Spain

†Correspondence:

Laura RUBIÓ, PhD

E-mail address: laura.rubio@iispv.cat

and

Maria-José MOTILVA, PhD

E-mail: motilva@tecal.udl.cat

Keywords: Hydroxytyrosol; hydroxytyrosol metabolites; atherosclerosis; ApoE$^{-/-}$ mice; human aortic endothelial cells

Abstract

The main aim of this work is to gain insight into the potential mechanisms of hydroxytyrosol (HT) and its main plasmatic metabolites (HTmet) that improve the endothelial function. Feeding ApoE$^{-/-}$ mice with 10 mg/kg/day of HT derivatives for 12 weeks significantly reduced E-selectin, VCAM-1, MCP-1, ICAM-1, and F4/80 expression compared with the control group in the isolated aorta. Further *in-vitro* mechanistic assays revealed that both HT and HTmet could reduce the adhesion of Jurkat-T-lymphocytes to human aortic endothelial cells at 1-5 µM, significantly greater reductions being observed with HTmet. This process appeared to be regulated by the MAPK pathway through the inactivation of p38δ, JNK1-3, CREB, AKT3, p53 and P70 S6 Kinase. We concluded that supplementation with HT precursors from olive oil might attenuate the initial step of atherosclerosis at a molecular level. The reduction of lymphocyte adhesion and the modulation of MAPK pathway by HTmet could explain this phenomenon.

1. Introduction

Cardiovascular diseases (CVD) contribute significantly to the mortality, morbidity and economic burden of illness and their prevention by dietary strategies has become a significant public health challenge. Chronic exposure to cardiovascular risk factors overwhelms the defence mechanisms of the vascular endothelium, hence compromising its integrity and ultimately initiating endothelial dysfunction (Chhabra, 2009). So, as this dysfunction is an initial and reversible step of atherosclerotic disease, inhibiting it is a possible approach to preventing CVD. Over recent years, the number of studies on food bioactive compounds as potential modulators of the endothelial function has risen (Rangel-Huerta, Pastor-Villaescusa, Aguilera, & Gil, 2015), given that the endothelium is exposed to these molecules or their biological metabolites in the bloodstream after absorption (Catalán et al., 2015).

Virgin olive oil (VOO), the leading source of fat in the Mediterranean diet, has been shown to protect against CVD (López-Miranda et al., 2010; Urpi-Sarda et al., 2012). This has mainly been related to its phenolic fraction. Hydroxytyrosol (HT) and its derivatives known as secoiridoids (SEC) are the most abundant and widely-studied olive oil phenolic compounds (OOPCs). Many beneficial effects have been attributed to HT. Its alleged anti-inflammatory, antioxidant, anti-cancer or endothelial and vascular functions have been studied in cells, animals, and humans (Echeverría, Ortiz, Valenzuela, & Videla, 2017). Recent animal studies showed that HT supplementation prevents metabolic alterations in desaturase activities, oxidative stress status and the n-3 long chain polyunsaturated fatty acid contents of the liver and extrahepatic tissues of mice fed a high-fat diet (HFD) (Valenzuela, Echeverria, et al., 2017). These metabolic alterations of the liver are regulated by activating the PPAR-α and Nrf2 transcription factors, along with the deactivation of NF-κB, induced in HFD-fed mice (Valenzuela,

Illesca, et al., 2017). In human studies, supplementing the diet with VOO rich in polyphenols improved the antioxidant and anti-inflammatory status and reduced the expression of cell adhesion molecules, compared with low-polyphenol VOO (Covas, 2007; López-Miranda et al., 2010). Other studies have shown that the endothelial function can be enhanced by consuming high-phenolic VOO in hypercholesterolemic (Juan Ruano et al., 2005) and hypertensive patients (Moreno-Luna et al., 2012; Valls et al., 2015).

After the daily consumption 5 mg of HT and its derivatives through 20 g of VOO, the dose required by the European Food Safety Authority (EFSA) for cardiovascular protection ("European Community, Council Regulation No. 432/2012 of 16 May 2012 establishing a list of permitted health claims made on foods, other than those referring to the reduction of disease risk, to children's development, health.," 2012), the native form of HT is not detected in plasma. It was observed that sulfation was the major pathway for HT metabolism in humans (Rubió et al., 2014). Therefore, the potential health benefits of OOPCs could be attributed to the biological activity of phase-II metabolites rather than the native form of HT.

In our previous study, a novel approach was developed using Caco-2 cells as bioreactors to enable a mixture of HT metabolites (HTmet) to be obtained with a 90% resemblance to human plasma after dietary doses of VOO (Catalán et al., 2015). In this study, HT metabolites were incubated with human aortic endothelial cells (HAEC), and a dose-dependent inhibition of the endothelial dysfunction biomarkers E-selectin, P-selectin, vascular cell adhesion molecule-1 (VCAM-1) and the intracellular cell adhesion molecule-1 (ICAM-1) was observed (Catalán et al., 2015). Additionally, a more significant effect of HT metabolites was observed in the reduction of the monocyte chemoattractant protein-1 (MCP-1/ CCL2) chemokine (Catalán et al., 2015).

These data provided evidence of the potential effect of HT phase-II metabolites in improving the endothelial dysfunction. However, the involvement of the circulating HT metabolites in the intracellular pathways of adhesion molecule secretion in the endothelial function has yet to be studied.

In the present work, the ApoE$^{-/-}$ mice model was supplemented with an olive phenolic extract rich in SEC at a nutritionally appropriate dose (10 mg/kg/day) to assess the improvement of the endothelial function in the initial steps of atherosclerosis. We conducted an *in-vitro* functional assay to study the mechanisms using physiological concentrations of HT and HTmet through the adhesion of lymphocytes to HAEC. For deeper insight into the molecular mechanisms, we evaluated the modulation of the mitogen-activated protein kinase (MAPK) family pathway and nuclear factor kappa-light-chain-enhancer of activated B cells (NF-κB). The potential post-transcriptional effects through the mRNA expression and stability of the VCAM-1, ICAM-1, E-selectin and MCP-1 molecules were also assessed.

2. Materials and Methods

2.1. Solvents and reagents

HT (99.5% purity) was purchased from Seprox Biotech (Madrid, Spain). Hydroxytyrosol-3'-O-sulfate was acquired from Toronto Research Chemicals Inc. (Toronto, Ontario, Canada) according to the method reported by Khymenets et al. (Khymenets et al., 2006). Methanol (HPLC-grade) and acetonitrile (HPLC-grade) were purchased from Scharlab (Barcelona, Spain) and orthophosphoric acid (85%) from Panreac (Barcelona, Spain). Milli-Q water was obtained from a Milli-Q water purification system (Millipore Corp., Medford, MA, USA).

2.2. Animals and diet

10 male and 10 female 6-week-old Apolipoprotein E knockout mice were purchased from Charles River Laboratories (Barcelona, Spain) and distributed between the control (4 male and 4 female) and secoiridoid (SEC) treatment groups (6 male and 6 female). The animals were maintained in regular temperature-controlled rooms (25 ± 2 °C) with controlled lighting (12 h light–dark cycles). The control mice received a standard isocaloric and isonitrogenous diet (Envigo, Harlan Laboratories, Madison, WI, USA). The SEC group diet was prepared weekly with a standard crushed diet mixed with Milli-Q water containing SEC extract with a dose equivalent to 10 mg of SEC/kg weight. The pellets were freeze-dried and stored at −20 ºC until use. The feed and animals were weighed every two days to adjust the weekly dose. After 12 weeks of treatment, the animals were kept in metabolic cages for 24 h to collect their urine and faeces. After that, they were anesthetized with isoflurane (IsoFlo, Veterinarian Esteve, Bologna, Italy) and sacrificed by exsanguination. Blood was collected in EDTA tubes (Vacutainer Tubes, BD, Franklin Lakes, NJ, USA) and plasma samples were obtained by centrifuging (3000 g, 10 min at 4ºC). The aorta was removed, rinsed with phosphate-buffered saline buffer and thoroughly cleaned of adventitial fat using surgical material under a stereoscopic microscope. The whole aorta was then immersed-fixed in 4% paraformaldehyde at 4ºC for 24 h.

The investigation was approved by the Animal Ethics Committee (7688) at the Universitat of Lleida (CEEA 17th February 2015) and the procedure was conducted in line with the guidelines of the European Communities Directive 2010/63/EU.

2.3. Preparation of the SEC phenolic extract

SEC extract from olive cake was prepared as previously reported (Khymenets et al., 2006) with some modifications. Briefly, 10 g of freeze-dried olive cake was mixed with 5 g of diatomaceous earth, and placed in an accelerated solvent extractor (ASE 100

Dionex, Sunnyvale, CA, USA). The solvent conditions were Ethanol/water (80:20), at 80ºC, 60% setting volume, and two 5-min static cycles. The ethanol was then eliminated by rotary evaporation. The aqueous extract was adjusted to pH=4 with acetic acid and then purified using the SPE method (OASIS HLB Elution cartridges 6 g, Waters, Milford, MA, USA). Cartridges were activated with 35 mL methanol, equilibrated with 40 mL of water pH=2, and loaded with 50 mL of ASE liquid extract., 30 mL of Milli-Q water was used to clean up followed by 20 mL of methanol 5% (v/v). Finally, the retained phenolic compounds were eluted with 60 mL of ethanol, and then rotary evaporated until the ethanol was totally evaporated (Buchi Rotavapor, DE, USA). An aliquot of the aqueous extract was analyzed by UPLC-MS/MS using the chromatographic method we reported previously (Rubió, Motilva, Macià, Ramo, & Romero, 2012). The phenolic composition of the extract used is available in **Supplementary Table 1**. To calculate the administered dose of 10 mg/kg weight of SEC, only 3,4-DHPEA-EDA was considered as the main secoiridoid derivate providing HT.

2.4. Analysis of phenolic compliance biomarkers in ApoE-/-

Urine samples collected before sacrifice were pre-treated using microelution solid-phase extraction (µSPE) (OASIS -HLB µElution plates 30 µm Waters, Milford, MA, USA) according to the method developed previously (Serra et al., 2013). The faeces were freeze-dried and pre-treated as previously described (López de las Hazas et al., 2016). The phenolic compounds in the urine and faeces were analyzed by Acquity Ultra-PerformanceTM liquid chromatography coupled to tandem MS as the detector system (UPLC-MS/MS) from Waters (Milford MA, USA), as reported in our previous study (López de las Hazas et al., 2016). The SRM conditions for the analysis of the phenolic metabolites by UPLC-ESI-MS/MS are shown in **Supplementary Table 2**.

2.5. Measurement of atherosclerotic lesion by oil red O staining

ApoE$^{-/-}$ mice aortas were stained with oil red to visualize neutral lipid accumulation. The immersion-fixed aortas were rinsed twice with 78% methanol and then submerged in 0.2% oil red solution (Sigma-Aldrich, Madrid, Spain) for 1 hour. After rinsing with 78% methanol, the aortic arch was cut open, and images of the oil red O-stained aortas were taken.

2.6. Histopathology staining

For Haematoxylin-Eosin, Masson trichrome and Alcian blue staining, the aortas were dehydrated following a cycle of different ethanol concentrations and then submerged in xylol. The samples were embedded in paraffin and sectioned into 5 µm and then deparaffinized and rehydrated in xylene and ethanol/water mixtures to perform the staining. Lesion areas were estimated using measurements from cryosections of the aortic base with the aid of the Photoshop CS6 (Adobe Systems Software, Ireland) and the ImageJ (Free software programmed in Java, public domain).

2.6.1. Haematoxylin-eosin

Haematoxylin-eosin staining was used to assess the integrity of the aorta. Hydrated histological cuts were incubated for 15 min with Harris's hematoxylin, washed with water and submerged in acid alcohol for 5 min. After rinsing with tap water, the samples were immersed in eosin (1%) for 5 min., and finally dehydrated by submerging for 5 min in ethanol, xylol, and xylol-eucalyptol (1:1) respectively to assemble the acrylic resin.

2.6.2. Masson Trichrome

Masson trichrome was used to study the collagen deposition and fibrosis in the arterial wall. Sections of rehydrated samples were submerged in Bouin's fixative (picric acid, formaldehyde and acetic acid (71,5/24/4,5 %) for 1 h at 56ºC. The samples were then washed with tap water until the yellowness disappeared. After that, the slides were submerged in Weigert Haematoxylin (haematoxylin 1% in ethanol + ferric clorure 20% in acid water) for 5 min, then washed with tap water and submerged in trichromic solution (light green with chromotropic and phosphotungstenic acid in water) for 10 min. After that, they were washed with distilled water and then immersed in light green colorant (2%) for 5 min. before being quickly washed with distilled water. Finally, the samples were dehydrated with ethanol (by submerging and taking out the samples), submerging with xylol (10min) and xylol-eucaliptol (1:1) for 10 min before mounting them.

2.6.3. Alcian Blue

Alcian blue staining was performed to assess the proteoglycan deposited on the aorta wall. Deparaffinized slide samples were submerged in Alcian blue (1%; pH=2,5 with acetic acid) for 30 min, before being washed firstly with tap water for 2 min and then with distilled water. After that, these samples were submerged in red nuclear (0.1%) for 5 min followed by 1 min of water rinsing. Finally, they were dehydrated by submerging them for 5 min in ethanol, xylol, and xylol-eucalyptol (1:1) respectively to assemble the acrylic resin.

2.7. Serum biomarkers

Serum total cholesterol (TC), triglycerides (TG), high-density lipoprotein cholesterol (HDLc) and glucose were measured by standardized methods using the Cobas Mira Plus autoanalyzer (Roche Diagnostics, Spain). Low-density lipoprotein

cholesterol (LDLc) was calculated with the Friedewald formula (Friedewald, Levy, & Fredrickson, 1972). TC, TG, HDLc, Glucose, and LDLc are expressed as mg/dL.

2.8. Immunohistochemistry assay of VCAM-1, E-selectin, MCP-1, ICAM-1, and F4/80 in mice aortic sections

VCAM-1, E-selectin, MCP-1, ICAM-1, and F4/80 were selected as representative adhesion molecules for the immunohistochemistry assay. Formalin-fixed aorta sections (5 µm) were obtained from the descending thoracic aorta, 3 mm distal to the left subclavian artery. The paraffin-embedded aorta was dewaxed and stained with anti-VCAM-1 and anti-E-selectin antibodies (Abcam ab134047 and ab185698 respectively; Cambridge, United Kingdom), ICAM-1 (sc-8439; Santa Cruz Biotechnology, Heidelberg, Germany) and F4/80 (MCA497RT; Bio-Rad Laboratories S.A., El Prat de Llobregat, Barcelona). The aorta samples were incubated in 10 mM citrate buffer in the microwave oven for 20 min for antigen retrieval or proteinase K 20 µg/mL at 37ºC for F4/80, before applying a 1:200 dilution of anti-VCAM-1, 1:100 dilutions of anti-E-selectin and ICAM-1, and 1:1000 dilution of anti-F4/80 overnight at 4ºC. To detect the MCP-1 antibody (Abcam ab25124; Cambridge, United Kingdom), the samples were incubated with the primary antibody (10 µg/mL) for 30 min. After washing with PBS, the samples were incubated in biotinylated rabbit anti-goat antibody for 60 min at 37°C. Staining was processed and visualized with ChemMate™ DAKO EnVision™ Detection Kit, Peroxidase/DAB, Rabbit/Mouse Code-Nr. K 5007 (Agilent Technologies, Madrid, Spain) according to the manufacturer's instructions.

Scoring of VCAM-1, E-selectin, MCP-1, ICAM-1, and F4/80 in the aorta was based on a semi-quantitative analysis previously used by Matsui R, et al. (Matsui et al., 2006). 40 photographs of immuno-stained Apo E-/- mouse aorta were taken under the microscope (x 40) and randomly shown to 3 observers without identifying the samples. Scores

(Grade 0 to 3) were given to the aortic tunica intima, media and adventitia according to the intensity of the staining (from 0 for low intensity to 3 for high intensity). The averages of the scores for each photograph given by the three observers were taken as the scores for the samples.

2.9. Biosynthesis, purification, and analysis of HT metabolites

Biosynthesis of the main plasmatic metabolites of HT was performed through Caco-2 cells as previously described (Catalán et al., 2015) to obtain a purified extract that resembled human plasma after VOO intake. Briefly, based on the biotransformation yield of HT into phase-II metabolites, after 24 h in T75 flasks, differentiated Caco-2 cells were exposed to 100 μM of HT. The metabolites obtained were HT sulfate (80%), homovanillic alcohol sulfate (10%) and, in a lesser proportion, HT glucuronides, and free HT. Before chromatographic analysis (see Section 2.4), the HT and its metabolites were isolated from the cell media using μSPE plates (Waters Corp., Milford, MA, USA) according to the previous study (Catalán et al., 2015). The phenolic composition was analyzed by an AcQuity UPLCTM coupled to a photodiode array detector detector and a triple quadrupole detector (TQD)TM mass spectrometer (Waters, Milford) with the chromatographic conditions previously reported (Catalán et al., 2015). HT and HT-3-O-sulphate were quantified with their calibration curves, and the other HTmet were tentatively quantified by using the calibration curve of HT. The calibration curves were constructed by using cellular medium free of HTmet.

2.10. Cell culture

2.10.1. Human aortic endothelial cells

HAEC (Cascade Biologics™, Portland, OR, USA) at the fifth passage were seeded on Nunclon™ Δ surface 12-well plates at a density of approximately 44×10^3 of viable cells/mL (for the mRNA assays), 96-well plates (for the adhesion assays) and 10-

cm dishes (for the MAPK proteome profiler and NF-κB activity assays). For the first 24 h, the cells were maintained in complete cell culture medium (CM) composed of M-200 medium supplemented with 2% (v/v) low-serum growth supplement, 10 mg/mL gentamicin, 0.25 mg/mL amphotericin B (purchased from Gibco by Life Technologies, Madrid, Spain), 100 U/mL penicillin and 100 mg/mL of streptomycin (from Biowest-Labclinics, Barcelona, Spain). The cells were grown to confluence at 37°C in a humidified incubator (Heracell 150; Madrid, Spain) with an atmosphere containing 5% CO2. The medium was replenished every 2 days with new CM. Viewed under an IMT2 microscope (Olympus, Barcelona, Spain), confluent monolayers displayed a typical monolayer phenotype of quiescent endothelial cells after 5 days in culture.

Experiments of time and dose-response were conducted to establish the final conditions of TNF-α (Calbiochem, Darmstadt, Germany) as a stimulant. The stock solutions used in the experiments were: 5 mM of HT (commercial; Seprox BIOTECH, Madrid, Spain) dissolved in sterile H_2O and tetraacetic mM of the purified solution of HT metabolites dissolved in methanol (Panreac, Madrid, Spain). Appropriate dilutions were prepared until the final concentrations for the culture media (0.5, 1, 2 and 5 μM) were obtained. To preempt cell cytotoxicity, methanol concentrations never exceeded 0.1% (v/v) in the culture media. Then, for the mRNA assays or adhesion assays, the HAECs were co-incubated with HT or HT metabolites at 0.5, 1, 2 and 5 μM and TNF-α (10 ng/mL), the respective vehicle control alone (sterile H_2O for HT or absolute methanol for HT metabolites) or TNF-α alone (10 ng/mL) for 24h. For the MAPK proteome profiler or NF-κB activity assays, HAECs were co-incubated with HT or HT metabolites 5 μM and TNF-α (10 ng/mL), blank (cells alone) or TNF-α alone (10 ng/mL) for 2 h.

The cytotoxicity effect of HT or HT metabolites on the HAECs was assessed with a Cytotoxicity Detection Kit LDH (Roche Applied Science, Mannheim, Germany) described in a previous study by the group (Catalán et al., 2015).

2.10.2. Jurkat T cell lymphocytes

Jurkat T cell lymphocytes were purchased from DSMZ GmbH (Braunschweig, Germany). These were cultured in an RPMI medium 1640 + Glutamax-I (Gibco, Spain) supplemented with 20% heat-inactivated foetal bovine serum (FBS) (PAA, Labclinics,) for the first 2 days, followed by 10% FBS + 100 U/mL penicillin and 100 mg/mL streptomycin for growth and the scheduled experiments. The Jurkat T cells were maintained until the cell-cell adhesion assays.

2.11. Functional Adhesion Assay

2.11.1. Calcein Labeling of Jurkat T Cells

Calcein acetoxymethyl ester (calcein-AM, Molecular Probes, Eugene, Oregon, USA) was used to fluorescently label the Jurkat T cells. Calcein is nonfluorescent, and the lipophilic molecule which is cleaved by endogenous esterases and the resulting product's fluorescence can be measured at 485 and 530 nm (excitation and emission wavelengths respectively). The Jurkat T cells were fluorescently labeled by incubating cells (5x106 cells/mL) with a final concentration of 5 µM of calcein-AM for 30 min at 37 °C and 5% CO2. After loading the calcein-AM, the cells were washed twice with an RPMI-1640 medium supplemented with 10% FBS to remove excess dye. The cells were finally resuspended in CM at a density of 2.5 x 10^6 cells/mL.

2.11.2. Cell-cell adhesion

HAECs were seeded until confluence in black 96-well tissue culture plates following the appropriate culture conditions with blank (cells alone), TNF-α (10ng/mL) or co-incubation with HT or HTmet (1, 2 and 5 µM) and TNF-α (10 ng/mL) for 24 h.

Then calcein-AM-labeled Jurkat T cells were cocultured (2.5 x 105 cells/well) with the HAEC monolayer for 1 h at 37°C in a humidified atmosphere with 5% CO_2. The nonadherent Jurkat T cells were removed from the HAEC monolayer by washing it twice with CM. The fluorescence intensity in each well of the culture plate was measured with the Synergy HT Fluorometer (BioTek Instruments, Alcobendas, Spain). The results are expressed as relative fluorescence units and SD (error bars).

2.12. Analysis of adhesion molecule mRNA expression by real-time quantitative reverse transcriptase polymerase chain reaction in HAEC

The HAECs were lysed with Lysis Buffer containing 1% 2-mercaptoethanol, and the total RNA was purified from the cells using a PureLink RNA Mini Kit from Ambion (Life Technologies, Madrid, Spain) according to the manufacturer's protocol. Total RNA was quantified using a Quant-it TM RNA Assay Kit and Qubit TM fluorometer (Invitrogen). Using the 2720 Thermal Cycler (Applied Biosystems), 0.5 µg of the total RNA was reverse transcribed to cDNA at 42°C for 50 min using random hexamers; SuperScript II reverse transcriptase and RNase Out (Invitrogen) according to the manufacturer's protocol. To determine the amounts of VCAM-1, E-selectin, ICAM-1 and MCP-1 mRNA, semiquantitative RT-PCR was performed using the ABI PRISM 7900 Detection System (Applied Biosystems) with the following profile: 95°C denaturing (20 s) with 40 cycles of extension at 95°C (1 s) and 60°C (20 s). Each sample was analyzed in triplicate, and the cycle threshold (Ct) was averaged from the values obtained in each reaction. The results of the VCAM-1, E-selectin, ICAM-1 and MCP-1 mRNA expression are reported as the increase (x-fold) using a $2 - \Delta\Delta Ct$ mathematical method. Glyceraldehyde-3-phosphate dehydrogenase (GAPDH; Applied Biosystems) was used as a housekeeping gene to normalize the results. TNF-α-activated endothelial cells were used as the calibrator in these experiments; their value was set at

1, and the other conditions were about this reference value. The results are expressed as the mean and SD (error bars) of the changes in VCAM-1, E-selectin, ICAM-1 and MCP-1 mRNA about TNF-α alone.

2.13. Stability of adhesion molecule mRNA after HT or HTmet incubation

Actinomycin D (Act D; Sigma-Aldrich, Spain) is an antineoplastic antibiotic isolated from Streptomyces sp bacteria that inhibits cell proliferation. Briefly, Act D is used as a transcription inhibitor because it inhibits the proliferation of cells in a non-specific way by forming a stable complex with double-stranded DNA (via deoxyguanosine residues), thus inhibiting DNA-primed RNA synthesis (Siboni et al., 2015). The half-life/stability of VCAM-1, ICAM-1, E-selectin and MCP-1 mRNA was measured after experimental incubations of HAECs. After 24 h of incubation with TNF-α (10 ng/mL) and HT or HTmet (5 µM), Act D (5 µg/mL) was added to the medium of each experiment condition. The incubation times with Act D were 0, 30, 60, 120 and 240 min. At these times, the cells were lysed to obtain the total RNA and processed following Section 2.9. The results were expressed as the mean and SD (error bars) of the changes in VCAM-1, ICAM-1, E-selectin and MCP-1 mRNA compared with time 0 min for each experimental condition.

2.14. MAPK proteome profiler array

In our experimental systems, we took advantage of the recently developed Human Phospho-MAPK Array from R&D Systems (Vitro, Madrid, Spain). It is a sensitive, semiquantitative and rapid tool for identifying the levels of phosphorylation of major mitogen-activated protein kinases (MAPKs): the extracellular-signal-regulated kinases (ERK1/ERK2), c-Jun N-terminal kinases (JNK 1–3), and different p38 MAPK isoforms (α, β, δ, and γ) and other intracellular kinases, such as Akt, glycogen synthase kinase (GSK-3), p70 S6 Kinase, TOR, p53 and CREB. This protein array technology

allows the screening of multiple proteins without the need to carry out various immunoprecipitation and western blot analyses.

Briefly, HAECs were rinsed with cold-PBS and immediately solubilized in 300 µL per 10-cm dish of Lysis Buffer 6 provided in Human Phospho-MAPK Array by rocking the lysates gently at 4˚C for 30 min. After micro-centrifuging at 14,000 x *g* for 5 min, the supernatants were transferred to a clean test tube, and sample protein concentrations were determined using the Bradford protein assay (See total cellular protein quantification section). The lysates were then stored at -80ºC until the MAPK proteome profiler array analysis.

The total cell lysates (200 µg of total protein per condition) were diluted and incubated according to the Human Phospho-MAPK Array manufacturer's instructions. The array data were developed using a ChemiDoc Image System and semi-quantified with Image Lab analysis software (both from Bio-Rad Laboratories S.A., Barcelona, Spain). Densitometry values of the different phosphorylated molecules were obtained by subtracting negative control values to avoid the background, as recommended by the manufacturer. The results are expressed as the mean pixel density and SD.

2.15. NF-B (p65) activity transcription factor assay

HAECs were washed twice with phosphate-buffered saline (PBS) purchased from Biowest (Labclinics, Barcelona, Spain). 300µL of hypotonic buffer (10mM 4-(2-hydroxyethyl)-1-piperazineethanesulfonic acid (HEPES), 0.1 mM EDTA, 0.1mM ethylene glycol tetraacetic acid (EGTA), 10 mM potassium chloride, 0.75 mM Spermidine, 0.15 mM Spermine, 0.5% skimmed milk, 1mM dithiothreitol (DTT) and one tablet of protease inhibitor cocktail per 10 mL of hypotonic buffer solution) was added to each 10 cm dish. The cells were scraped with the cell lifter, and all the contents were transferred to a microcentrifuge tube. These were then aspirated and expelled with

a syringe BD Plastipak 305501 1ml Syringe with 26G x 0.5 (Bellés Diagnòstic i Investigació, S.L., Tarragona, Spain) 10 times to assure all the content was properly lysed. The samples were centrifuged at 16,000 x g for 10 min at 4ºC. The supernatants containing the cytoplasmic fraction were kept at -80ºC for future analysis.

50 µL of extraction buffer (20 mM HEPES, 1 mM EDTA, 1 mM EGTA, 0.42 M sodium chloride; NaCl, 25% Glycerol, 1mM DTT and one tablet of protease inhibitor cocktail per 10 mL of extraction buffer solution) was added to the pellets and maintained at 4ºC for 45 min and mix-vortexed vigorously every 15 min. Then the samples were centrifuged at 16,000 x g for 1 h at 4ºC. The supernatants containing the nuclear extracts were stored at -80ºC until the quantification of the total cellular protein content and detection of NF-κB.

Activation of the NF-κB (p65) from the nuclear extracts (5 µg of nuclear protein per condition, as recommended by the manufacture's protocol) was measured using the NF-κB (p65) Transcription Factor Assay Kit from Cayman Chemical (Vitro, Madrid, Spain). The activity of NF-κB p65-DNA binding was depicted as relative optical density (OD) at 450 nm / µg of protein.

2.16. Total cellular protein quantification

To adjust the same quantity of protein for all the experimental conditions, the total cellular protein concentration from the cell lysates (nuclear lysates for NF-kB determination and total cellular lysates for MAPK proteome profiler) was determined using the Bradford protein assay from Bio-Rad with bovine serum albumin (BSA). A range of concentrations of BSA was used as the calibration standards for the protein assay. The absorbance was measured at 595 nm.

2.17. Statistical Analyses

All the experiments were performed at least twice, and each incubation condition was set up from three to eight replicates. One-way analysis of variance (ANOVA) followed by Bonferroni's posthoc test was used for multiple comparisons. A value of $p<0.05$ was considered statistically significant. A requisite for the analytical quality of the model was the control of several aspects involved in the cellular process and analytical performance of measurements. All the results were analyzed with the Statistical Package for the Social Sciences (SPSS) software (version 22.0). The results are expressed as the mean (SD).

3. Results

3.1. Phenolic compliance biomarkers

HT and its metabolites were measured in 24 h-urine and faeces in ApoE$^{-/-}$ mice at the end of the experiment to monitor the phenolic compliance of the group supplemented with SEC extract. A significant increase in HT phase-II metabolites after SEC supplementation was observed in urine, the main metabolites detected being HT sulfate and homovanillic acid sulfate, confirming that the complex forms of OOPCs are mainly absorbed as HT (**Supplementary Table 3**).

3.2. Serum lipid and glucose biomarkers

There were no significant differences in the biochemical parameters of TC, TG, HDLc, LDLc and glucose in ApoE$^{-/-}$ mice fed with 10 mg SEC/kg/day compared with the control group fed with the standard diet (**Table 1**). Moreover, no intra-group or inter-group changes were observed between males or females.

3.3. Atherosclerotic lesion in ApoE$^{-/-}$ mice aorta

The atherosclerotic plaques were analyzed in the entire aorta by Oil-Red-O staining in ApoE$^{-/-}$ mice after control and SEC treatment. The results revealed that after 12 weeks

of SEC supplementation or control diet, none of the groups presented visible atherosclerotic lesions (**Figure 1A**).

The atherosclerotic lesion in the aorta was further investigated more accurately by haematoxylin-eosin, Masson trichrome and Alcian blue staining for the presence of specific cell types and factors that could define the stages in the development of lesions. The histopathology staining revealed no significant differences between the control and the SEC treatment (**Supplementary Figure 1**). No differences were observed between males and females.

3.4. Immunohistochemistry assay of VCAM-1, E-selectin, MCP-1, ICAM-1, and F4/80 in ApoE$^{-/-}$ in isolated mice aorta

Given the absence of atherosclerotic plaque, VCAM-1, E-selectin, MCP-1, and ICAM-1expression as molecular markers of endothelial dysfunction and F4/80 expression as macrophage marker were studied by immunohistochemistry in ApoE$^{-/-}$ aorta sections. Semi-quantitative analysis showed that the aortas from the SEC group had less staining of E-selectin, MCP-1, and ICAM-1 in the tunica intima, media and adventitia compared with the control group (p<0.05; **Figures 1B, D, and E**). VCAM-1 and F4/80 staining was also less intensive in the SEC group in the tunica intima and adventitia compared with the control group (p<0.05; **Figure 1C and F**) but not in the tunica media. The positive-staining cells for F4/80 were considered to be infiltrating macrophages.

3.5. HAEC cytotoxicity

For the *in-vitro* assays with HAEC, the native form of HT and a mixture of its plasmatic metabolites (HTmet) obtained as previously reported (Catalán et al., 2015) were tested at physiological concentrations. There was no evidence of HAEC cytotoxicity following the co-incubation of HT or HTmet at different concentrations (1, 2 and 5 µM) and TNF-

α (10 ng/mL) for 24 h. No difference was measured in the activity of LDH release compared with the TNF-α (10 ng/mL) treatment alone, confirming that HT and HTmet are not cytotoxic at the concentrations and times tested. These results were reported in a previous study by Catalán *et al*. (Catalán et al., 2015).

3.6. Effect of HT or HTmet on Lymphocyte Cell Adhesion to HAECs

Qualitatively, very few lymphocyte Jurkat T cells adhered to untreated HAECs (**Figures 2A and B**) whereas a considerable number of cells adhered to HAECs after the TNF-α (10ng/mL) treatment (**Figure 2C**). Lymphocyte adhesion to HAECs co-incubated with HT or HTmets at 1, 2 and 5 µM with TNF-α appeared to decrease compared with the condition of HAECs only treated with TNF-α. Co-incubation of HTmets and TNF-α seemed to decrease greatly compared with HT at all concentrations tested (**Figure 2G, H** and **I** *versus* **D, E**, and **F**).

These qualitatively results seem to be confirmed by the cell fluorescence images, which revealed that exposure of HAECs to HTmet at 1, 2 and 5 µM reduced the adhesion of the Jurkat T cells significantly by 11.0, 10.3 and 54.2% respectively compared with TNF-α alone (**Figure 2K**). HT also reduced the adhesion of lymphocytes to HAECs significantly at 1, 2 and 5 µM, but to a lesser extent of 5.1, 11.3 and 3.5% respectively (**Figure 2J**). Comparing the HT and HTmet treatments, as observed qualitatively, the HTmet produced a greater percentage reduction of lymphocyte adhesion than HT at 1 and 5 µM (**Figure 2K)**.

3.7. Effect of HT or HTmet on E-selectin, ICAM-1, VCAM-1 and MCP-1 mRNA expression by HAECs

In our previous study (Catalán et al., 2015), after observing a significant decrease in E-selectin, ICAM-1, VCAM-1, P-selectin and MCP-1 protein secretion after the exposure of the HAECs to HT or HTmet, we aimed to study the intracellular mechanisms in

greater depth and determine the mRNA expression of these molecules (**Figure 3**). At lower concentrations (0.5, 1 and 2 µM), neither HT, HTmets nor modified mRNA levels compared with TNF-α alone. As shown in **Figures 3A** and **B**, HTmet only reduced E-selectin and VCAM-1 mRNA expression significantly at 5 µM, by approximately 44 and 40% ($p<0.05$), respectively. HTmets also reduced ICAM-1 mRNA expression by 32%, but this reduction was not statistically significant (**Figure 3C**). We also observed a decrease in MCP-1 mRNA expression after HT exposure at the highest concentration of 5 µM but in a non-significant way (**Figure 3D**).

3.8. Effect of HT and HTmet on VCAM-1, ICAM-1, E-selectin and MCP-1 mRNA kinetic stability in HAEC cells using the RT-PCR assay

The results from the kinetic measurement of mRNA stability from 0 to 240 min in HAEC cells, showed that VCAM-1, ICAM-1, E-selectin and MCP-1 mRNA levels fell progressively from the starting point (time 0 min) and reached the minimum level at 120 min and remained stable until 240 min under all test conditions (**Supplementary Figure 2**). No significant differences between HT and HTmet in TNF-α, VCAM-1 and E-selectin mRNA levels were observed at 5 µM. The pattern for HT was similar to TNF-α alone in stabilizing VCAM-1, ICAM-1, E-selectin and MCP-1 mRNA expression (**Supplementary Figures 2A, B, C, and D**, respectively), and showed no differences between any molecules at any time. However, HTmet stabilized ICAM-1 mRNA at 120 min and MCP-1 mRNA at 30 and 120 min, compared with TNF-α alone ($p<0.05$; **Supplementary Figures 2B and D**). HTmet stabilized MCP-1 mRNA expression at 30 min more than HT ($p<0.05$; **Supplementary Figure 2D**).

3.9. Effect of HT and HTmet on the MAPK family and NF-κB activity in HAEC cells

After performing the proteome array, we identified at the same time the activation status of all three major MAPKs: ERK1/ERK2, JNK 1-3 and different p38 MAPK isoforms

(α, β, δ, and γ) as well as other intracellular kinases, such as Akt, GSK-3, p70 S6 Kinase, TOR, p53 and CREB in whole-cell lysates from HAECs.

The transcription factors Akt1, Akt2, Akt pan, GSK-3α/β, GSL-3β, HSP27, JNK1, MSK2, RSK1, RSK2, and TOR showed no significant modulation after HAEC exposure to HT or HTmet at 5 µM (data not shown).

The representative array results of the spot membranes are shown in **Figures 4A** (Blank), **4B** (TNF-α 10 ng/mL), **4C** (HT 5µM + TNF-α 10 ng/mL) and **4D** (HTmet 5 µM + TNF-α 10 ng/mL). **Figure 4E** shows the pixel density of the transcription factors that HT or HTmet were able to reduce compared with the TNF-α condition. The results indicate that, compared with the TNF-α condition, at 5µM, HT and HTmet significantly decreased CREB (11.09 and 11.99% respectively), JNK pan (JNK 1-3; 18.5 and 27.55% respectively), p38δ (23.73 and 33.73% respectively) and p70 S6 Kinase (28.64 and 32.20 % respectively). As observed, the percentage reductions of those molecules were greater with HTmet than the HT condition, but those differences were not significant. HT and HTmet also reduced the ERK1 (6.87 and 5.39% respectively), MKK3 (11.63 and 39.87% respectively), MKK6 (2.18 and 31.23% respectively) and p38β (18.79 and 17.64% respectively) molecules compared with the TNF-α condition. However, these reductions were not significant.

The HT condition reduced significantly p38α (21.66%) and p38γ (29.48%) compared with TNF-α ($p<0.05$) while HTmet did not reduce those molecules. The latter reduced Akt3 (31.10%), JNK2 (45.28%) and p53 (27.22%) compared with TNF-α alone significantly ($p<0.05$). However, HT not reduce those molecules.

The NF-κB p65 activation showed that TNF-α (10 ng/mL) increased the activity 10-fold compared with blank (control condition) demonstrating a proper stimulation of the cells ($p<0.05$). HT or HTmet at 5 µM showed no significant difference in p65-NF-κB activation compared with TNF-α alone (**Supplementary Figure 3**).

4. Discussion

The improvement of the endothelial function with OOPCs as a way of protecting against atherosclerosis has been described in several human studies (Moreno-Luna et al., 2012; J. Ruano et al., 2005; Valls et al., 2015). Considering the great metabolism these compounds undergo when absorbed, in this study we report novel potential mechanisms of main plasmatic HT phase-II metabolites for attenuating the initial steps of atherosclerosis for the first time using a translational approach with *in-vitro* and *in-vivo* experiments.

Initially, the effect of OOPCs on the endothelial function of ApoE $^{-/-}$ mice was tested by supplementing their diet with a phenolic extract rich in SEC. The compliance of the group with the diet supplemented with the SEC extract was corroborated by measuring 24 h-urine and faeces in the ApoE$^{-/-}$ mice at the end of the experiment. A significant increase in the main HT phase-II metabolites (HT sulfate and homovanillic acid sulfate) was observed in the urine of mice after supplementing their diet with SEC. Those results were corroborated by Khymenets et al. in humans who demonstrated that HT is bioavailable and can be recovered in the urine as HT sulfate (Khymenets et al., 2016). Given that a standard diet was used instead of a high-fat diet, atherosclerotic development was very limited in both the SEC and control groups after 12 weeks. The high-fat diet significantly accelerates atherogenesis in ApoE $^{-/-}$ model and induces the formation of the advanced lesions containing necrotic cellular cores and fibrous caps as well as a large plaque (Xue-Mei et al., 2017). In this study, we used a standard diet as

we aimed to test the potential role of a diet supplemented with nutritionally appropriate doses of OOPCs without any pro-inflammatory diet, given that a high-fat diet represents a toxic proinflammatory stimulus rather than a low and chronic inflammatory state in animals (Okada et al., 2013). Due to this and the low doses of OOPCs administered, no differences were found in the plasmatic lipid profile, lipid accumulation, collagen and proteoglycan deposition and the integrity of the aorta in SEC group compared with the control group in the ApoE $^{-/-}$ mice model. These results are in line with previous studies conducted by Acín S et al. (Acín et al., 2006) who found no significant changes in HDLc, paraoxonase, apolipoprotein B or triglyceride levels although they observed a decrease in apolipoprotein A-I and an increase in the total cholesterol, atherosclerotic lesion areas and circulating monocytes expressing Mac-1 after HT administration in ApoE$^{-/-}$ deficient mice fed with a chow diet for 10 weeks. The levels of LDLc observed in our study seems to be higher in the SEC group than in the control group, however, this difference did not reach statistical significance. May be increasing the number of animals may decrease the SD, a result also observed by Acín S *et al*. where LDLc where significantly higher in polyphenol group compared to control group (Acín et al., 2006). Notwithstanding, when we assessed the molecular levels of the VCAM-1, E-selectin, MCP-1, and ICAM-1 protein expression in the tunica intima, media, and adventitia of isolated mice aortas after 12 weeks of treatment, these molecules decreased significantly in the SEC group compared with the control group, suggesting attenuation at the molecular level in the initial steps of atherosclerosis. In the same line, Katsarou et al. observed that the phenolic constituents of VOO reduced the E-selectin and VCAM-1 molecules in the aorta of rats (Katsarou et al., 2015). Moreover, the detection of F4/80 (a macrophage marker) expression in the isolated aortas of the ApoE^{-} $^{/-}$ mice showed that macrophages were widely distributed in the lesions of the aortic

roots in the control group and in SEC group F4/80 where significantly decreased showing less macrophages distributed in the aorta section. Result within accordance to Lin et al., where observed an increase of the number of macrophages present within lesions compared to the control group (Lin et al., 2015).

To study the implication of HT and its biological metabolites on the intracellular pathways of VCAM-1, ICAM-1, E-selectin and MCP-1 molecules secretion, we performed an experiment with HAECs using a mix of HTmet at doses similar to that previously detected in human plasma after the ingestion of VOO (Rubió et al., 2014). For this purpose, we chose an adhesion functional assay simulating the physiological conditions of the first stages of atherosclerosis when leukocytes (monocytes and/or lymphocytes) are attracted to the endothelial cells due to the secretion of endothelial dysfunction molecules secreted by inflammatory cytokines, such as TNF-α (Libby, Ridker, & Hansson, 2011). The functional study showed that both HT and HTmet reduced the adhesion of the lymphocytes to HAECs at all concentrations tested, with significantly greater reductions with HTmet. These results suggest an active role of the circulating HTmet in attenuating the lymphocyte adhesion process. No previous studies have conducted a functional adhesion assay with OOPCs but similar experiments performed with other antioxidant compounds, such as alpha-tocopherol, also inhibited the adhesion of Jurkat T lymphocytes to HAECs (Catalán et al., 2012; Koga, Claycombe, & Meydani, 2002).

After the functional study, in order to gain insight into the intracellular mechanisms of VCAM-1, ICAM-1, E-selectin, and MCP-1, we assessed their mRNA expression and stability, and the modulation of the MAPK family and NF-κB transcription pathways. All mechanistic *in-vitro* assays performed in this study are

summarized in **Table 2**. This table reflects greater overall effects with HTmet rather than the native form of HT and also shows different pathway modulation.

The reduction of E-selectin, ICAM-1, and VCAM-1 mRNA expression by HTmet agreed with our previous experiments in which we reported that the protein expression of these molecules was significantly inhibited by HTmet in HAECs (Catalán et al., 2015). The present mechanistic studies have shown that the mRNA and protein reduction by HTmet could be regulated by the MAPK pathway but not by the NF-κB pathway. Particularly, HTmet significantly reduced the phosphorylation of p38δ, JNK1-3, CREB, AKT3, p53 and P70 S6 Kinase. These results suggest that VCAM-1, ICAM-1, and E-selectin could be regulated by HTmet at the beginning of the pathway through the inhibition of the MAPK transcription factors with a consequent inhibition of the mRNA and protein secretion (**Figure 5**).

On the other hand, the HTmet had no effects on MCP-1 mRNA expression, indicating that HTmet could inhibit MCP-1 protein expression at the post-transcriptional level. Hence, MCP-1 synthesis could be governed by multiple factors, such as post-transcriptional modifications occurred in the nucleus, the cytoplasm or both, or by post-translational modifications produced at the cytoplasm level. A possible post-transcriptional mechanism of MCP-1 regulation that could explain that disagreement on mRNA and protein secretion shown recently by Tomé-Carneiro et al. (Tomé-Carneiro et al., 2017) could be also be explained by small noncoding RNAs (micro-RNAs; miRNA). Indeed, it has been reported that the increase in TNF-α downregulates miR-122 causes the upregulation of MCP-1 (Li et al., 2016). Another study performed on human umbilical vein endothelial cells (HUVEC) indicated that the decrease in miR-495 upregulates MCP-1 (Liu et al., 2015). Other miRNA targets, such as miR-146a (Yang et al., 2011) or miR-467b (Tian et al., 2012) downregulate MCP-1,

which could be decreased by HTmet incubation. Moreover, possible MCP-1 post-translational modifications could be due by sulfated modifications on chemokine receptors on tyrosine residues in their N-terminal regions, the initial site of binding to MCP-1 chemokine ligands. Tan *et al.* demonstrated that the interaction with the sulfated N-terminus of chemokine receptor type 2 (CCR2) destabilizes the dimerization interface of inactive dimeric MCP-1, thus inducing dissociation from the active monomeric state (Tan et al., 2013).

Regarding the effects of HT, the results showed that the native structure of HT could reduce some molecules of the MAPK pathway significantly (p38 α, δ and γ, CREB, P70 S6 Kinase and JNK1-3). However, the results indicated a less efficient modulation of the MAPK pathway compared with HTmet, which could be the reason for the non-modulation of the mRNA expression of the adhesion molecules (**Figure 5**). Despite that, in our previous study, we observed a reduction in the protein secretion of E-selectin, P-selectin, ICAM-1, and VCAM-1 adhesion molecules by HT (Catalán et al., 2015), suggesting other HT mechanisms apart from those studied here. In agreement with our results, Dell'Agli *et al*. showed the effects of HT on the reduction of E-selectin protein secretion, with no changes in E-selectin mRNA expression in HUVEC (Dell'Agli et al., 2006), whereas they did not present any possible mechanism to explain this controversy. Differential mRNA expression-protein studies have demonstrated the poor correlation between mRNA and protein expression levels (Koussounadis, Langdon, Um, Harrison, & Smith, 2015). Indeed, only 40% of the variation in protein concentration can be explained by the abundance of mRNA (Vogel & Marcotte, 2012). To explain the remaining 60% of the variation, gene ontology theme enrichment analysis indicated that the genes with high correlations between RNA-protein expressions were mainly involved in maintaining cellular processes and structural

properties (Gry et al., 2009). Therefore, we suggest a possible different mechanism than HTmet related to post-transcriptional or post-translational modifications by HT to explain the discordance observed in this study between the mRNA and protein secretion of adhesion molecules with HT treatment.

As we observed in our study, HAECs represent a direct target for studying the action of bioactive molecules once these are absorbed in the blood stream where they probably regulate the adhesion protein expression by transcriptional and posttranscriptional mechanisms. The data obtained provide new mechanistic insights that could partly explain the improvement in the endothelial dysfunction by OOPCs observed in humans, highlighting that the HT biological metabolites circulating in plasma after absorption could be the main contributors to this effect. Thus, our results complement the hypothesis in Muto *et al.* that "*olive oil phenols also act through pathways others than NF-κB*" (Muto et al., 2015) which is corroborated by our study and others (Aparicio-Soto et al., 2016).

In conclusion, the supplementation with OOPCs at nutritionally relevant doses showed a mild attenuation of the initial steps of atherosclerosis through the reduction of endothelial dysfunction biomarkers E-selectin, VCAM-1 and MCP-1 in the tunica intima, media, and adventitia of the aorta of ApoE $^{-/-}$ mice fed without a pro-inflammatory diet. This inhibition could be mainly explained by the action of the plasmatic circulating HTmet as they were more efficient than the native structure of HT at plasmatic physiological concentrations in the reduction of lymphocyte adhesion and the modulation of the MAPK pathway in endothelial cells. Thus, for the first time, the present study reveals the plasmatic circulating metabolites of HT could have an important role in preventing the endothelial dysfunction, indicating that this process might be regulated by the MAPK pathway.

Conflict of interest

The authors declare no conflict of interest.

5. Acknowledgements

This work was partly supported by state grant: The MEFOPC Project (Subprojects AGL2012-40144-C03-02 and AGL2012-40144-C03-03) from the Spanish Ministry of Education and Science (*Ministerio de Educación y Ciencia*). We wish to acknowledge the support of the *Institut d'Investigació Sanitària Pere Virgili* (IISPV) and the *Centre Tecnològic de Nutrició i Salut* (CTNS), Reus, Spain and the University of Lleida through the M-C. López de las Hazas grant and the L. Rubió Sara Borrell postdoctoral grant (CD14/00275). And the Ú. Catalán Pla estratègic de recerca i innovació en salut (PERIS) post-doctoral grant (SLT002/16/00239; Catalunya, Spain). NFOC-Salut group is a consolidated research group of Generalitat de Catalunya, Spain (2014 SGR 873).

6. Bibliography

Acín, S., Navarro, M. A., Arbonés-Mainar, J. M., Guillén, N., Sarría, A. J., Carnicer, R., … Osada, J. (2006). Hydroxytyrosol administration enhances atherosclerotic lesion development in apo E deficient mice. *Journal of Biochemistry*, *140*(3), 383–91. https://doi.org/10.1093/jb/mvj166

Aparicio-Soto, M., Sánchez-Hidalgo, M., Cárdeno, A., Rosillo, M. Á., Sánchez-Fidalgo, S., Utrilla, J., … Alarcón-de-la-Lastra, C. (2016). Dietary extra virgin olive oil attenuates kidney injury in pristane-induced SLE model via activation of

HO-1/Nrf-2 antioxidant pathway and suppression of JAK/STAT, NF-κB and MAPK activation. *The Journal of Nutritional Biochemistry*, *27*, 278–88. https://doi.org/10.1016/j.jnutbio.2015.09.017

Catalán, Ú., Fernández-Castillejo, S., Pons, L., Heras, M., Aragonés, G., Anglès, N., … Solà, R. (2012). Alpha-Tocopherol and BAY 11-7082 Reduce Vascular Cell Adhesion Molecule in Human Aortic Endothelial Cells. *Journal of Vascular Research*, *49*(4), 319–328. https://doi.org/10.1159/000337466

Catalán, Ú., López de Las Hazas, M.-C., Rubió, L., Fernández-Castillejo, S., Pedret, A., de la Torre, R., … Solà, R. (2015). Protective effect of hydroxytyrosol and its predominant plasmatic human metabolites against endothelial dysfunction in human aortic endothelial cells. *Molecular Nutrition & Food Research*. https://doi.org/10.1002/mnfr.201500361

Chhabra, N. (2009). Endothelial dysfunction – A predictor of atherosclerosis. *Internet Journal of Medical Update*, *4*(1).

Covas, M.-I. (2007). Olive oil and the cardiovascular system. *Pharmacological Research*, *55*(3). https://doi.org/10.1016/j.phrs.2007.01.010

Dell'Agli, M., Fagnani, R., Mitro, N., Scurati, S., Masciadri, M., Mussoni, L., … Caruso, D. (2006). Minor components of olive oil modulate proatherogenic adhesion molecules involved in endothelial activation. *Journal of Agricultural and Food Chemistry*, *54*(9), 3259–64. https://doi.org/10.1021/jf0529161

Echeverría, F., Ortiz, M., Valenzuela, R., & Videla, L. A. (2017). Hydroxytyrosol and Cytoprotection: A Projection for Clinical Interventions. *International Journal of Molecular Sciences*, *18*(5), 930. https://doi.org/10.3390/ijms18050930

European Community, Council Regulation No. 432/2012 of 16 May 2012 establishing a list of permitted health claims made on foods, other than those referring to the reduction of disease risk, to children's development, health. (2012). *Official Journal of the European Union, L136*, 1–40. Retrieved from https://www.fsai.ie/uploadedFiles/Reg432_2012.pdf

Friedewald, W. T., Levy, R. I., & Fredrickson, D. S. (1972). Estimation of the concentration of low-density lipoprotein cholesterol in plasma, without use of the preparative ultracentrifuge. *Clinical Chemistry*, *18*(6), 499–502.

Gry, M., Rimini, R., Strömberg, S., Asplund, A., Pontén, F., Uhlén, M., & Nilsson, P. (2009). Correlations between RNA and protein expression profiles in 23 human cell lines. *BMC Genomics*, *10*, 365.

Katsarou, A. I., Kaliora, A. C., Papalois, A., Chiou, A., Kalogeropoulos, N., Agrogiannis, G., & Andrikopoulos, N. K. (2015). Serum lipid profile and inflammatory markers in the aorta of cholesterol-fed rats supplemented with extra virgin olive oil, sunflower oils and oil-products. *International Journal of Food Sciences and Nutrition*, *66*(7), 766–73. https://doi.org/10.3109/09637486.2015.1088936

Khymenets, O., Crespo, M. C., Dangles, O., Rakotomanomana, N., Andres-Lacueva, C., & Visioli, F. (2016). Human hydroxytyrosol's absorption and excretion from a nutraceutical. *Journal of Functional Foods*, *23*, 278–282. https://doi.org/10.1016/j.jff.2016.02.046

Khymenets, O., Joglar, J., Clapés, P., Parella, T., Covas, M.-I., & de la Torre, R. (2006). Biocatalyzed Synthesis and Structural Characterization of Monoglucuronides of Hydroxytyrosol, Tyrosol, Homovanillic Alcohol, and 3-(4′-

Hydroxyphenyl)propanol. *Advanced Synthesis & Catalysis*, *348*(15), 2155–2162. https://doi.org/10.1002/adsc.200606221

Koga, T., Claycombe, K., & Meydani, M. (2002). Homocysteine increases monocyte and T-cell adhesion to human aortic endothelial cells. *Atherosclerosis*, *161*(2), 365–74. Retrieved from http://www.ncbi.nlm.nih.gov/pubmed/11888519

Koussounadis, A., Langdon, S. P., Um, I. H., Harrison, D. J., & Smith, V. A. (2015). Relationship between differentially expressed mRNA and mRNA-protein correlations in a xenograft model system. *Scientific Reports*, *5*, 10775.

Li, C., Deng, M., Hu, J., Li, X., Chen, L., Ju, Y., … Meng, S. (2016). Chronic inflammation contributes to the development of hepatocellular carcinoma by decreasing miR-122 levels. *Oncotarget*, *7*(13), 17021–34.

Libby, P., Ridker, P. M., & Hansson, G. K. (2011). Progress and challenges in translating the biology of atherosclerosis. *Nature*, *473*(7347), 317–25.

Lin, Y., Bai, L., Chen, Y., Zhu, N., Bai, Y., Li, Q., … Liu, E. (2015). Practical assessment of the quantification of atherosclerotic lesions in apoE−/− mice. *Molecular Medicine Reports*, *12*(4), 5298–5306. https://doi.org/10.3892/mmr.2015.4084

Liu, D., Zhang, X.-L., Yan, C.-H., Li, Y., Tian, X.-X., Zhu, N., … Han, Y.-L. (2015). MicroRNA-495 regulates the proliferation and apoptosis of human umbilical vein endothelial cells by targeting chemokine CCL2. *Thrombosis Research*, *135*(1), 146–54.

López-Miranda, J., Pérez-Jiménez, F., Ros, E., De Caterina, R., Badimón, L., Covas, M. I., … Yiannakouris, N. (2010). Olive oil and health: Summary of the II

international conference on olive oil and health consensus report, Jaén and Córdoba (Spain) 2008. *Nutrition, Metabolism and Cardiovascular Diseases*, *20*(4), 284–294. https://doi.org/10.1016/j.numecd.2009.12.007

López de las Hazas, M.-C., Piñol, C., Macià, A., Romero, M.-P., Pedret, A., Solà, R., … Motilva, M.-J. (2016). Differential absorption and metabolism of hydroxytyrosol and its precursors oleuropein and secoiridoids. *Journal of Functional Foods*, *22*, 52–63. https://doi.org/10.1016/j.jff.2016.01.030

Matsui, R., Xu, S., Maitland, K. A., Mastroianni, R., Leopold, J. A., Handy, D. E., … Cohen, R. A. (2006). Glucose-6-phosphate dehydrogenase deficiency decreases vascular superoxide and atherosclerotic lesions in apolipoprotein E(-/-) mice. *Arteriosclerosis, Thrombosis, and Vascular Biology*, *26*(4), 910–6. https://doi.org/10.1161/01.ATV.0000205850.49390.3b

Moreno-Luna, R., Muñoz-Hernandez, R., Miranda, M. L., Costa, A. F., Jimenez-Jimenez, L., Vallejo-Vaz, A. J., … Stiefel, P. (2012). Olive oil polyphenols decrease blood pressure and improve endothelial function in young women with mild hypertension. *American Journal of Hypertension*, *25*(12), 1299–304. https://doi.org/10.1038/ajh.2012.128

Muto, E., Dell'Agli, M., Sangiovanni, E., Mitro, N., Fumagalli, M., Crestani, M., … Caruso, D. (2015). Olive oil phenolic extract regulates interleukin-8 expression by transcriptional and posttranscriptional mechanisms in Caco-2 cells. *Molecular Nutrition & Food Research*, *59*(6), 1217–21. https://doi.org/10.1002/mnfr.201400800

Okada, Y., Yamaguchi, K., Nakajima, T., Nishikawa, T., Jo, M., Mitsumoto, Y., … Itoh, Y. (2013). Rosuvastatin ameliorates high-fat and high-cholesterol diet-

induced nonalcoholic steatohepatitis in rats. *Liver International*, *33*(2), 301–311. https://doi.org/10.1111/liv.12033

Rangel-Huerta, O., Pastor-Villaescusa, B., Aguilera, C., & Gil, A. (2015). A Systematic Review of the Efficacy of Bioactive Compounds in Cardiovascular Disease: Phenolic Compounds. *Nutrients*, *7*(7), 5177–5216. https://doi.org/10.3390/nu7075177

Ruano, J., Lopez-Miranda, J., Fuentes, F., Moreno, J. A., Bellido, C., Perez-Martinez, P., … Pérez Jiménez, F. (2005). Phenolic content of virgin olive oil improves ischemic reactive hyperemia in hypercholesterolemic patients. *Journal of the American College of Cardiology*, *46*(10). https://doi.org/10.1016/j.jacc.2005.06.078

Ruano, J., Lopez-Miranda, J., Fuentes, F., Moreno, J. A., Bellido, C., Perez-Martinez, P., … Pérez Jiménez, F. (2005). Phenolic content of virgin olive oil improves ischemic reactive hyperemia in hypercholesterolemic patients. *Journal of the American College of Cardiology*, *46*(10), 1864–8. https://doi.org/10.1016/j.jacc.2005.06.078

Rubió, L., Farràs, M., de La Torre, R., Macià, A., Romero, M.-P., Valls, R. M., … Motilva, M.-J. (2014). Metabolite profiling of olive oil and thyme phenols after a sustained intake of two phenol-enriched olive oils by humans: Identification of compliance markers. *Food Research International*, *65*(PA), 59–68.

Rubió, L., Motilva, M.-J., Macià, A., Ramo, T., & Romero, M.-P. (2012). Development of a phenol-enriched olive oil with both its own phenolic compounds and complementary phenols from thyme. *Journal of Agricultural and Food Chemistry*, *60*(12), 3105–12. https://doi.org/10.1021/jf204902w

Serra, A., Rubió, L., Macià, A., Valls, R.-M., Catalán, U., de la Torre, R., & Motilva, M.-J. (2013). Application of dried spot cards as a rapid sample treatment method for determining hydroxytyrosol metabolites in human urine samples. Comparison with microelution solid-phase extraction. *Analytical and Bioanalytical Chemistry*, *405*(28), 9179–92. https://doi.org/10.1007/s00216-013-7322-2

Siboni, R. B., Nakamori, M., Wagner, S. D., Struck, A. J., Coonrod, L. A., Harriott, S. A., … Berglund, J. A. (2015). Actinomycin D Specifically Reduces Expanded CUG Repeat RNA in Myotonic Dystrophy Models. *Cell Reports*, *13*(11), 2386–94.

Tan, J. H. Y., Ludeman, J. P., Wedderburn, J., Canals, M., Hall, P., Butler, S. J., … Stone, M. J. (2013). Tyrosine sulfation of chemokine receptor CCR2 enhances interactions with both monomeric and dimeric forms of the chemokine monocyte chemoattractant protein-1 (MCP-1). *The Journal of Biological Chemistry*, *288*(14), 10024–34.

Tian, G.-P., Chen, W.-J., He, P.-P., Tang, S.-L., Zhao, G.-J., Lv, Y.-C., … Tang, C.-K. (2012). MicroRNA-467b targets LPL gene in RAW 264.7 macrophages and attenuates lipid accumulation and proinflammatory cytokine secretion. *Biochimie*, *94*(12), 2749–55.

Tomé-Carneiro, J., Crespo, M. C., García-Calvo, E., Luque-García, J. L., Dávalos, A., & Visioli, F. (2017). Proteomic evaluation of mouse adipose tissue and liver following hydroxytyrosol supplementation. *Food and Chemical Toxicology : An International Journal Published for the British Industrial Biological Research Association*, *107*(Pt A), 329–338. https://doi.org/10.1016/j.fct.2017.07.009

Urpi-Sarda, M., Casas, R., Chiva-Blanch, G., Romero-Mamani, E. S., Valderas-Martínez, P., Arranz, S., … Estruch, R. (2012). Virgin olive oil and nuts as key

foods of the Mediterranean diet effects on inflammatory biomarkers related to atherosclerosis. *Pharmacological Research*, *65*(6), 577–583. https://doi.org/10.1016/j.phrs.2012.03.006

Valenzuela, R., Echeverria, F., Ortiz, M., Rincón-Cervera, M. Á., Espinosa, A., Hernandez-Rodas, M. C., … Videla, L. A. (2017). Hydroxytyrosol prevents reduction in liver activity of Δ-5 and Δ-6 desaturases, oxidative stress, and depletion in long chain polyunsaturated fatty acid content in different tissues of high-fat diet fed mice. *Lipids in Health and Disease*, *16*(1), 64. https://doi.org/10.1186/s12944-017-0450-5

Valenzuela, R., Illesca, P., Echeverría, F., Espinosa, A., Rincón-Cervera, M. Á., Ortiz, M., … Videla, L. A. (2017). Molecular adaptations underlying the beneficial effects of hydroxytyrosol in the pathogenic alterations induced by a high-fat diet in mouse liver: PPAR-α and Nrf2 activation, and NF-κB down-regulation. *Food Funct.*, *8*(4), 1526–1537. https://doi.org/10.1039/C7FO00090A

Valls, R.-M., Farràs, M., Suárez, M., Fernández-Castillejo, S., Fitó, M., Konstantinidou, V., … Solà, R. (2015). Effects of functional olive oil enriched with its own phenolic compounds on endothelial function in hypertensive patients. A randomised controlled trial. *Food Chemistry*, *167*. https://doi.org/10.1016/j.foodchem.2014.06.107

Vogel, C., & Marcotte, E. M. (2012). Insights into the regulation of protein abundance from proteomic and transcriptomic analyses. *Nature Reviews. Genetics*, *13*(4), 227–32.

Xue-Mei, L., Jie, C., Xuan, D., Xiao-Xing, L., Chun-Lin, H., & Yu-Jie, L. (2017). Changes in $CD4^{+}CD25^{+}$ Tregs in the pathogenesis of atherosclerosis in $ApoE^{-/-}$

mice. *Experimental Biology and Medicine*, 153537021668982. https://doi.org/10.1177/1535370216689826

Yang, K., He, Y. S., Wang, X. Q., Lu, L., Chen, Q. J., Liu, J., … Shen, W. F. (2011). MiR-146a inhibits oxidized low-density lipoprotein-induced lipid accumulation and inflammatory response via targeting toll-like receptor 4. *FEBS Letters*, *585*(6), 854–60.

Figure captions

Figure 1. Representative Immunohistochemistry staining for E-selectin, VCAM-1 and MCP-1 in ApoE-/- mouse aortic sections. (A) Representative images of oil red stained transversal-sections from Control and SEC Apo E-/- mice aorta samples. Aorta semi-quantitative analysis of E-selectin (B), VCAM-1 (C), MCP-1 (D), ICAM-1 (**E**), and F4/80 (**F**) staining (see Materials and Methods Section). The data are expressed as the mean (standard deviation; SD) of the scores obtained for The effect tunica intima, media and adventitia of the aortic wall for each molecule stained. *p <0.05 SEC compared with the Control group.

Figure 2. Images of the adhesion of Jurkat T cells to TNF-α-treated HAEC under microscope (X4 and X10) in the experiments (A-I). The conditions for this study were: A) hydroxytyrosol (HT) vehicle control (H_2O); B) HT metabolites (HTmet) vehicle control (MetOH); C) TNF-α (10 ng/mL); co-incubation of D-F) HT or G-I) HTmet (1, 2 and 5 µM) and TNF-α (10 ng/mL). J and K represent the relative fluorescence units

(RFU) corresponding to each condition in the experiment.*p < 0.05 versus TNF-α alone. †p<0.05 compared between HT and HTmet at the same concentration.

Figure 3. The effect of HT or HTmet (0.5, 1, 2 and 5 μM) on E-selectin, VCAM-1, ICAM-1 and MCP-1 mRNA expression in HAECs stimulated by TNF-α (10ng/mL) for 24h. A) The effect of HT or HTmet on E-selectin mRNA expression. B) The effect of HT or HTmet on VCAM-1 mRNA expression. C) The effect of HT or HTmet on ICAM-1 mRNA expression. D) The effect of HT or HTmet on MCP-1 mRNA expression. The results are the mean and the standard deviations (SD; error bars) of two independent experiments where each set of experimental conditions was run in triplicate. *p < 0.05 versus TNF-α alone.

Figure 4. The effect of hydroxytyrosol (HT) and HT metabolites (HTmet) on the phosphorilation status of all three major families of mitogen-activated protein kinases (MAPKs): the extracellular signal-regulated kinases (ERK 1/2), c-Jun N-terminal kinases (JNK 1-3) and different p38 isoforms (α/β/δ/γ) in human aortic endothelial cells. A-D) The templates showing the location of MAPK antibodies spotted onto the membrane of Human Phospho-MAPK Array Kit: A) blank cells; B) TNF-α (10ng/mL); C) HT (5μM) + TNF-α (10ng/mL); D) HTmet (5μM) + TNF-α (10ng/mL). E) The densitometry values of the different phosphorylated molecules were obtained by subtracting negative control values in order to avoid the background, as recommended by manufacturer. The data are expressed as the mean of the pixel density and SD (error bars). *p < 0.05 versus TNF-α (10 ng/mL).

Figure 5. Graphic representation summarizing the suggested intracellular mechanisms of the action of hydroxytyrosol (HT) and its main plasmatic metabolites (HTmet) in the attenuation of atherosclerosis. † $p<0.001$ versus HT.

Supplementary Figure 1. Different staining of sections of ApoE$^{-/-}$ mice aorta after the control and secoiridoid (SEC) treatments to measure the atherosclerotic burden. A) Alcian blue staining (proteoglycan deposition); B) Hematoxylin eosin staining (integrity of aorta); C) Masson tricromic staining (fibrosis).

Supplementary Figure 2. The effect of HT and HTmet on VCAM-1, ICAM-1, E-selectin and MCP-1 mRNA stabilization in HAECs using the RT-PCR assay. The HAECs were incubated with TNF-α alone (10 ng/ml), HT or HTmet (5 μM) and TNF-α (10 ng/mL) for 24h. The incubation times with Act D were 0, 30, 60, 120 and 240 min. At these times, the cells were lysed to obtain the total RNA. The data were normalized using the values obtained from the GAPDH (housekeeping gene), and are the mean of two separate experiments run in triplicate. The error bars show the SD. *p < 0.05 *versus* TNF-αalone (10 ng/mL). †p<0.05 HTmet compared with HT at the same concentration.

Supplementary Figure 3. The effect of HT and HTmet on the activity of NF-κB p65-DNA binding in human aortic endothelial cells. The data are expressed as the relative optical density (OD) at 450 nm / μg of protein.

Graphical abstract

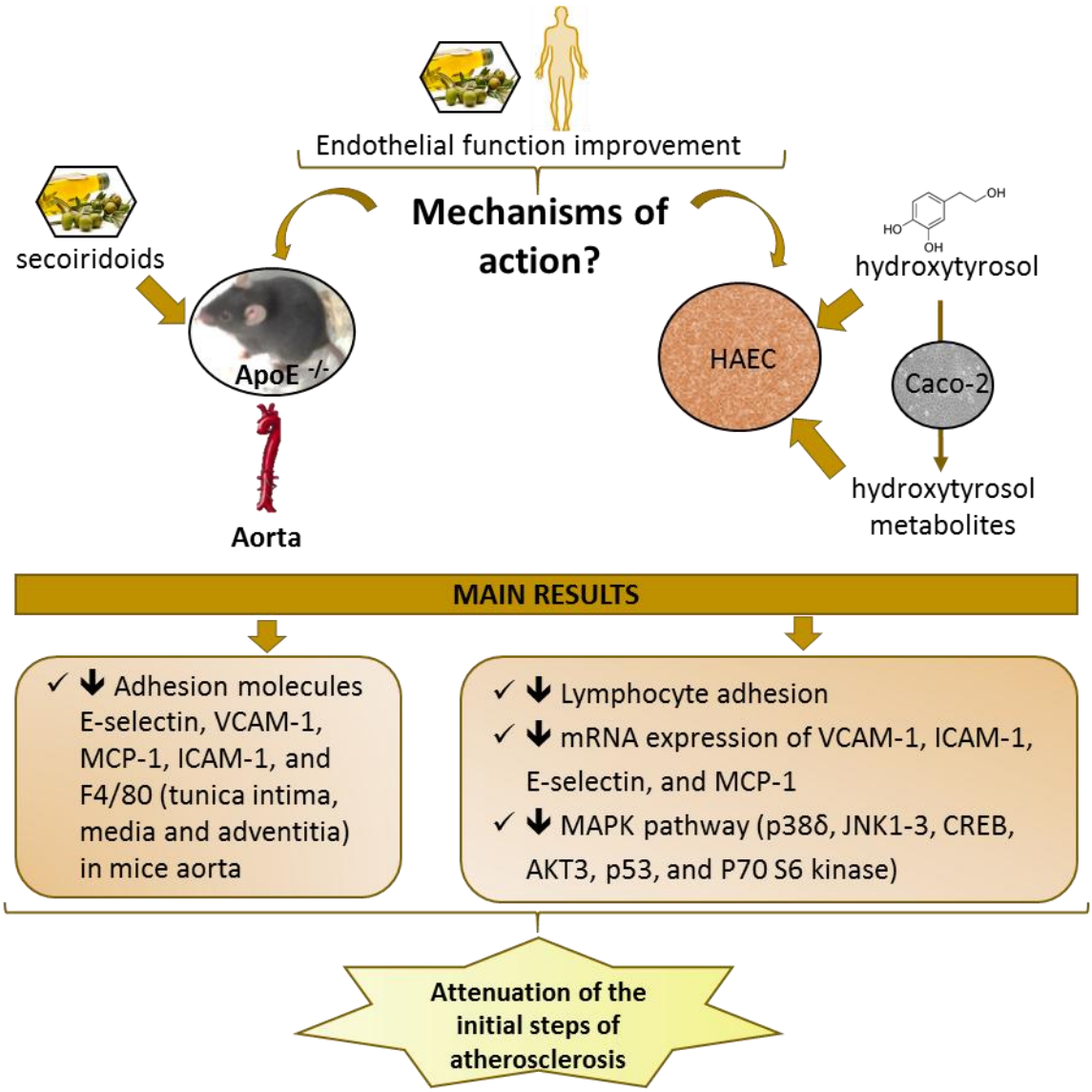
Endothelial function improvement
Mechanisms of action?
secoiridoids
ApoE -/-
Aorta
hydroxytyrosol
HAEC
Caco-2
hydroxytyrosol metabolites
MAIN RESULTS
✓ ↓ Adhesion molecules E-selectin, VCAM-1, MCP-1, ICAM-1, and F4/80 (tunica intima, media and adventitia) in mice aorta
✓ ↓ Lymphocyte adhesion
✓ ↓ mRNA expression of VCAM-1, ICAM-1, E-selectin, and MCP-1
✓ ↓ MAPK pathway (p38δ, JNK1-3, CREB, AKT3, p53, and P70 S6 kinase)
Attenuation of the initial steps of atherosclerosis

957

958

Table 1

Table 1. Biochemical parameters in ApoE$^{-/-}$ mice serum after the experiment.

	ApoE $^{-/-}$ control group		ApoE $^{-/-}$ secoiridoid group			
	Males (n=4)	Females (n=4)	Males (n=6~~7~~)	Females (n=6~~4~~)		
Biochemical parameters (mg/dL)	Mean (SD)	Mean (SD)	Mean (SD)	Mean (SD)	*p* males between groups	*p* females between groups
Glucose	245.3 (17.95)	261.3 (24.93)	268.86 (24.45)	291.25 (20.69)	>0.050	>0.050
Total Cholesterol	294.50 (48.01)	260.23 (32.77)	400.72 (70.59)	297.10 (34.94)	>0.050	>0.050
Triglycerides	92.98 (11.66)	76.54 (23.82)	97.49 (19.84)	67.98 (20.54)	>0.050	>0.050
HDL	21.14 (2.39)	13.80 (2.57)	22.95 (4.91)	10.62 (2.83)	>0.050	>0.050
LDL	254.84 (49.48)	231.19 (31.16)	358.35 (64.82)	272.95 (28.98)	>0.050	>0.050

HDL, high-density lipoprotein; LDL, low-density lipoprotein

LDL was calculated by Friedewald formula.

One-way analysis of variance (ANOVA) followed by Bonferroni's posthoc test was used for multiple comparisons. A value of $p<0.05$ was considered statistically significant.

Table 2

Table 2. Summary of the results obtained after hydroxytyrosol and hydroxytyrosol metabolites incubation.

	Concentrations tested (μM)		Hydroxytyrosol	Hydroxytyrosol metabolites
MAPK pathway	5		↓p38 α*, p38δ*, p38γ*, JNK1-3*, CREB* and P70 S6 Kinase* (↓p38β, Akt3, p53 and ERK1)	↓p38 δ*, JNK1-3*, CREB*, Akt3*, P70 S6 Kinase* and p53* (↓p38β and ERK1)
NF-KB pathway	5		↓	NE
mRNA quantification	0.5, 1, 2 and 5	VCAM-1	NE	↓ 5μM* (↓ 0.5-2 μM)
		ICAM-1	NE	↓ 1-5 μM
		E-selectin	NE	↓ 5μM*
		P-selectin	-	-
		MCP-1	↓ 5μM	↑ 2-5μM*
mRNA stability	5	VCAM-1	NE	NE
		ICAM-1	NE	↑120 min*
		E-selectin	NE	NE
		P-selectin	-	-
		MCP-1	NE	↑30 and 120 min*
Protein secretion	1, 2, 5 and 10	VCAM-1	↓ 1-10μM*	↓ 2-10μM*
		ICAM-1	↓ 1-10μM*	↓ 2-10μM*
		E-selectin	↓ 1-10μM*	↓ 2-10μM*
		P-selectin	↓ 1-10μM*	↓ 2-10μM*
		MCP-1	NE	↓ 5-10μM*
Cell-cell adhesion	1, 2 and 5		↓ 1-5μM*	↓ 1-5μM*†

NE, no effects.
* $p<0.05$ *versus* TNF-α alone.
† $p<0.001$ *versus* HT.

Supplemental Table 1. Composition of SEC extract (mg/L) obtained after pressurized liquid extraction from olive cake followed by SPE purification.

Compound	mg/L of extract
Tyrosol	625.3 ± 60.0
Hydroxytyrosol	4779.2 ± 101.5
Hydroxytyrosol Acetate	70.2 ± 1.9
Elenolic acid	1529.6 ± 11.5
p-HPEA-EDA	0.3 ± 0.02
3,4-DHPEA-EDA	3358.6 ± 185.4
Ligstroside derivate	177.1 ± 2.1
p-HPEA-EA	1.2 ± 0.1
Oleuropein derivate	78.1 ± 3.2
3,4-DHPEA-EA	33.5 ± 2.4
Oleuropein	109.5 ± 2.6

p-HPEA-EDA, dialdehydic form of elenolic acid linked to tyrosol; 3,4-DHPEA-EDA, dialdehydic form of elenolic acid linked to hydroxytyrosol; *p*-HPEA-EA, aldehydic form of elenolic acid linked to tyrosol; 3,4-DHPEA-EA, isomer of oleuropein aglycone.

Values are expressed as mean ± SD (n=3).

Supplemental Table 2

Supplemental Table 2. SRM conditions for the analysis of hydroxytyrosol metabolites by UPLC-MS/MS.

Phenolic compound	Quantification (SRM_1)			Identification (SRM_2)			Standard in which has been quantified
	SRM	Cone voltage (V)	Collision energy (eV)	SRM	Cone voltage (V)	Collision energy (eV)	
Hydroxytyrosol	153 > 123	35	10	153 > 95	35	25	Hydroxytyrosol
Hydroxytyrosol sulfate	233 > 153	40	15	233 > 123	40	25	Hydroxytyrosol-3-*O*-sulfate
Hydroxytyrosol disulfate	313 > 233	40	10	313 > 153	40	30	Hydroxytyrosol-3-*O*-sulfate
Hydroxytyrosol-3-*O*-glucuronide	329 > 153	40	20	329 > 123	40	25	Hydroxytyrosol
Hydroxytyrosol-4-*O*-glucuronide	329 > 153	40	20	329 > 123	40	25	Hydroxytyrosol
Homovanillic alcohol	167 > 152	35	15	167 > 122	35	25	Hydroxytyrosol
Homovanillic alcohol sulphate	247 > 167	40	15	247 > 152	40	25	Hydroxytyrosol
Homovanillic alcohol glucuronide	343 > 167	40	20	343 > 152	40	35	Hydroxytyrosol
Homovanillic acid	181 > 137	25	10	181 > 122	25	15	Hydroxytyrosol
Homovanillic acid sulphate	261 > 181	40	15	261 > 137	40	25	Hydroxytyrosol
Homovanillic acid glucuronide	357 > 181	40	20	357 > 137	40	30	Hydroxytyrosol
Hydroxytyrosol acetate sulphate	275 > 153	35	15	275 > 123	35	30	Hydroxytyrosol
Elenolic acid	241 > 139	30	15	241 > 127	30	20	Hydroxytyrosol
Elenolic acid sulphate	321 > 241	40	15	321 > 139	40	20	Oleuropein
Elenolic acid glucuronide	417 > 241	40	15	417 > 139	40	20	Oleuropein
Oleuropein	539 > 377	35	15	539 > 275	35	20	Oleuropein
Oleuropein glucuronide	715 > 539	55	15	715 > 377	55	25	Oleuropein
Oleuropein aglycone sulfate	457 > 377	40	15	457 > 275	40	20	Oleuropein
Oleuropein aglycone glucuronide	553 > 377	40	15	553 > 377	40	20	Oleuropein
Methyl oleuropein aglycone sulfate	471 > 391	40	15	391 > 275	40	20	Oleuropein
Oleuropein aglycone derivate 1	555 > 523	40	15	555 > 275	40	25	Oleuropein
Oleuropein aglycone derivate 2	571 > 539	40	15	571 > 377	40	25	Oleuropein
Catechol	108.9 > 90.9	40	15	-	-	-	Catechol
Phenylacetic acid	135 > 91	20	5	-	-	-	*p*-Hydroxyphenylacetic acid
Hydroxyphenylacetic acid	151 > 107	20	10	-	-	-	*p*-Hydroxyphenylacetic acid
Hydroxyphenylacetic acid sulphate	231 > 151	20	20	231 > 107	20	25	*p*-Hydroxyphenylacetic acid
Hydroxyphenylacetic acid glucuronide	327 > 151	20	15	327 > 107	20	25	*p*-Hydroxyphenylacetic acid
Dihydroxyphenylacetic acid	167 > 123	20	10	-	-	-	3,4-Dihydroxyphenylacetic acid
Hydroxybenzoic acid	137 > 93	30	15	-	-	-	*p*-Hydroxyphenylacetic acid
Protocatechuic acid	153 > 109	45	15	-	-	-	Hydroxytyrosol
Hydroxyphenylpropionic acid	165 > 121	20	10	-	-	-	3-(4-Hydroxyphenyl)propionic acid
Hydroxyphenylpropionic acid sulphate	245 > 165	35	15	245 > 121	35	20	3-(4-Hydroxyphenyl)propionic acid
Dihydroxyphenylpropionic acid	181 > 137	20	15	-	-	-	3-(4-Hydroxyphenyl)propionic acid
Hippuric acid	178 > 134	40	10	-	-	-	Hippuric acid
Hydroxyhippuric acid	194 > 100	40	10	-	-	-	Hippuric acid

Supplemental Table 3

Supplemental Table 3. Phenolic compliance biomarkers in 24h-urine **(**µM) and feces at the end of the ApoE$^{-/-}$ study.

Urine biomarkers (µMol)	ApoE$^{-/-}$ male		ApoE$^{-/-}$ female	
	Control	SEC	Control	SEC
HT	0.00±0.00	0.05±0.02*	0.00±0.00	0.06±0.03*
Homovanillic alcohol	0.01±0.00	0.05±0.03*	0.03±0.00	0.08±0.03*
HT S	0.00±0.00	0.18±0.07*	0.00±0.00	0.14±0.05*
Homovanillic alcohol S	0.04±0.01	0.06±0.01	0.04±0.03	0.10±0.04
Homovanillic acid S	0.34±0.03	0.41±0.06*	0.24±0.01	0.60±0.28*
HT acetate S	0.00±0.00	0.01±0.00	0.00±0.00	0.05±0.04
Fecal biomarkers	ApoE$^{-/-}$ male		ApoE$^{-/-}$ female	
(nmol/g fresh feces)	Control	SEC	Control	SEC
Phenylacetic ac	23.66±11.07	39.86±16.25*	6.75±4.72	9.97±7.71*
OHphenylacetic ac	93.85±17.40	159.9±34.78*	125.3±16.63	138.5±17.36*
HT	n.d.	11.64±6.12	n.d.	14.15±10.4
OHPhenylpropionic ac	14.16±3.08	32.01±7.44*	18.89±3.81	30.20±7.00*
diOHphenylacetic ac	n.d.	20.08±18.4	n.d.	8.09±6.43
Hippuric ac	67.37±10.55	110.1±84.6*	45.89±25.25	85.67±73.19
Tyrosol S	3.03±2.06	17.0±10.0*	n.d.	21.82±25.00
OHphenylacetic ac S	39.47±41.47	124.0±68.3*	21.10±13.00	49.03±21.71*
HT S	n.d.	30.67±57.50	n.d.	12.70±4.05
OHPhenylpropionic ac S	175.9±12.6	260.8±196.7	194.7±140.3	162.2±133.35*
Homovanillic ac S	39.61±47.42	143.1±44.0*	18.16±12.33	28.62±22.47*
DiOHPhenylpropionic ac S	n.d.	17.74±32.02	n.d.	36.11±86.98
HT acetate S	n.d.	40.56±31.42	n.d.	16.85±9.12
Catechol S	25.23±17.48	31.51±11.21*	11.76±8.19	84.48±47.55*
Methyl catechol S	7.17±14.34	101.2±34.79*	n.q.	76.46±67.60
Coumaric acid S	26.85±1.98	37.38±4.52*	21.67±8.92	40.00±10.47*

n.d., not detected; n.q., not quantified; HT, hydroxytyrosol; OH, hydroxy; S, sulfate; G, glucuronide; ac, acid.

Results are expressed as mean ± s.d.

* P<0.05 One-Way Anova *vs* control

Figure 1

Click here to download high resolution image

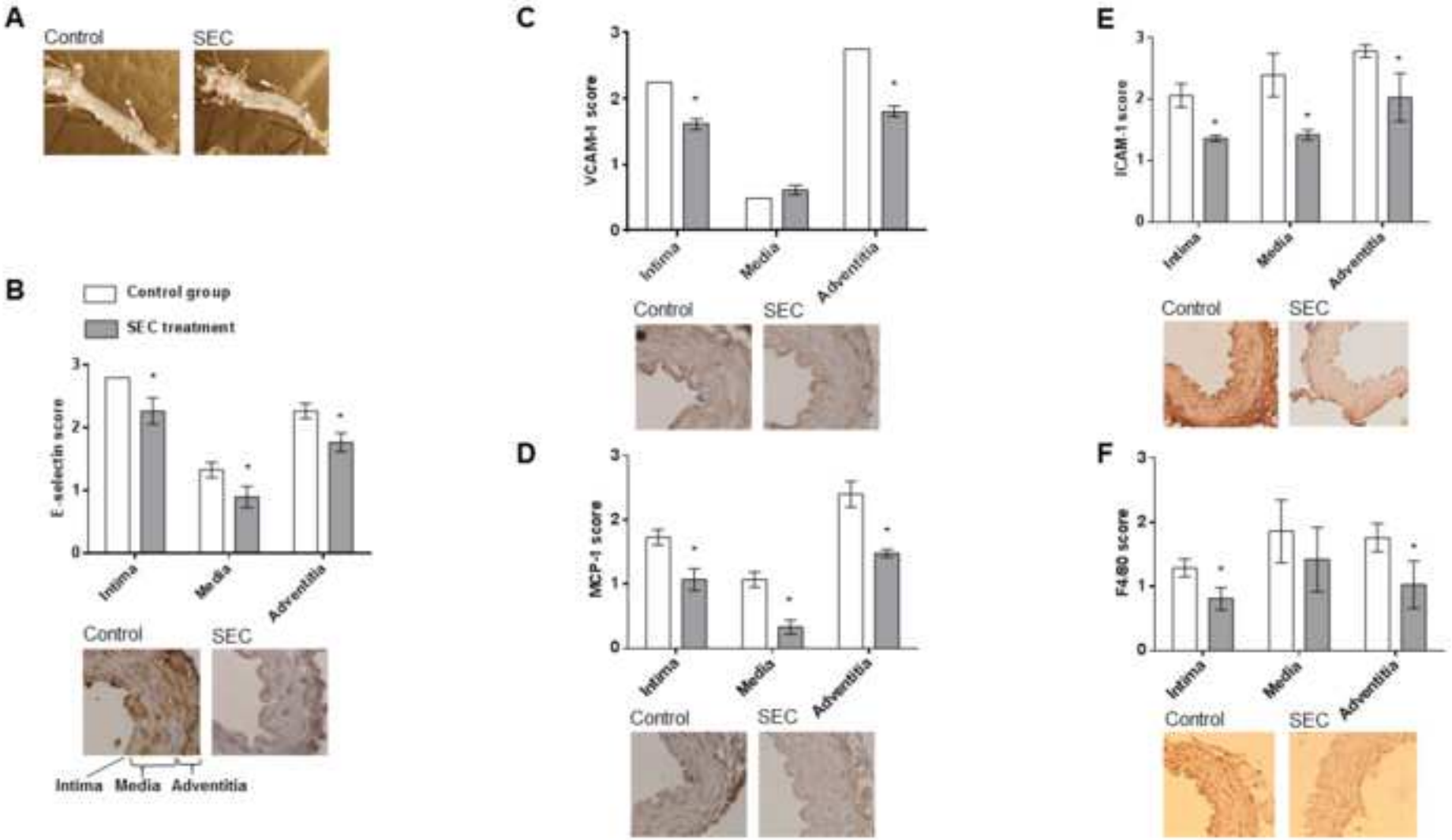

Figure 2

Click here to download high resolution image

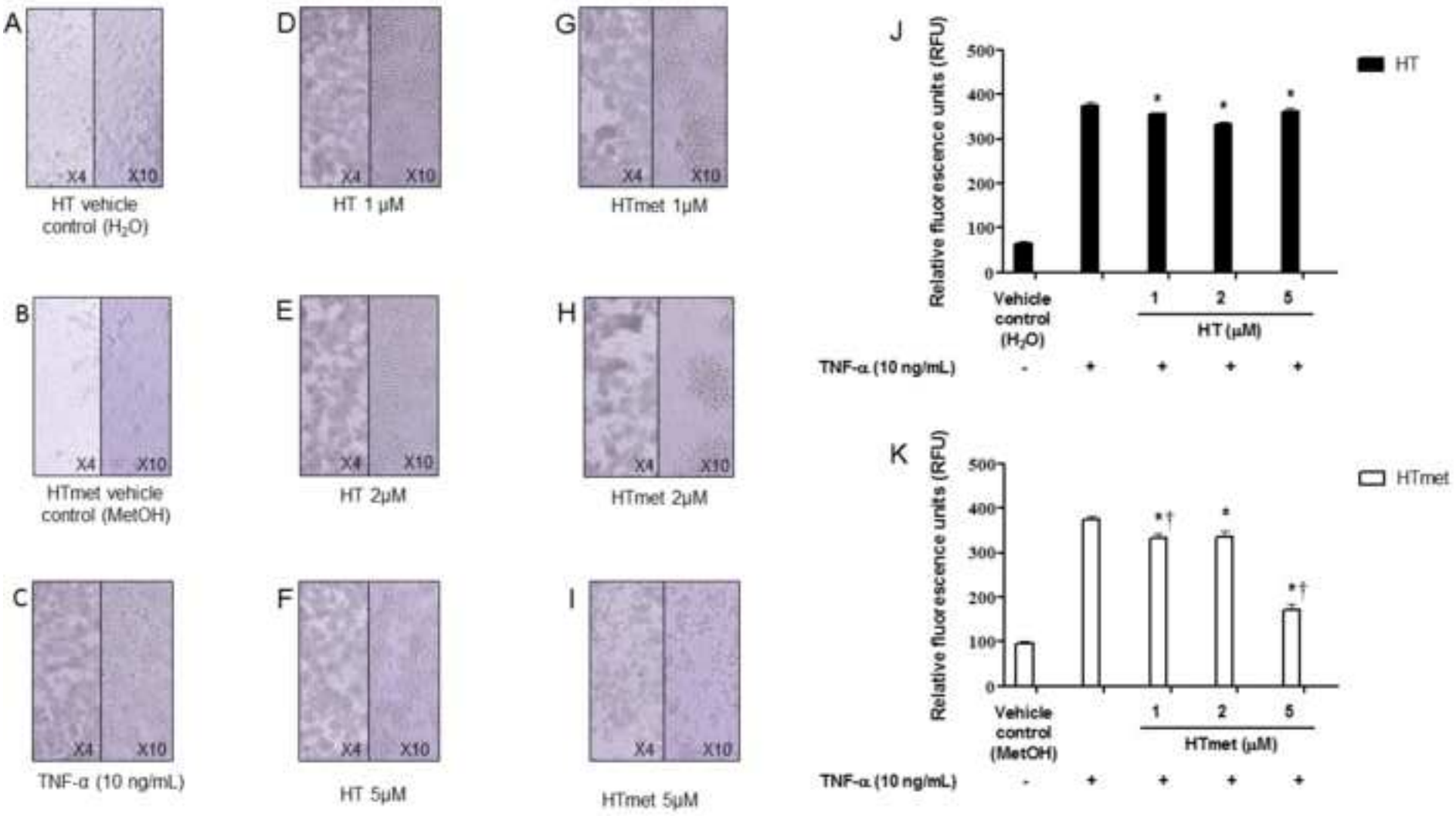

Figure 3

Click here to download high resolution image

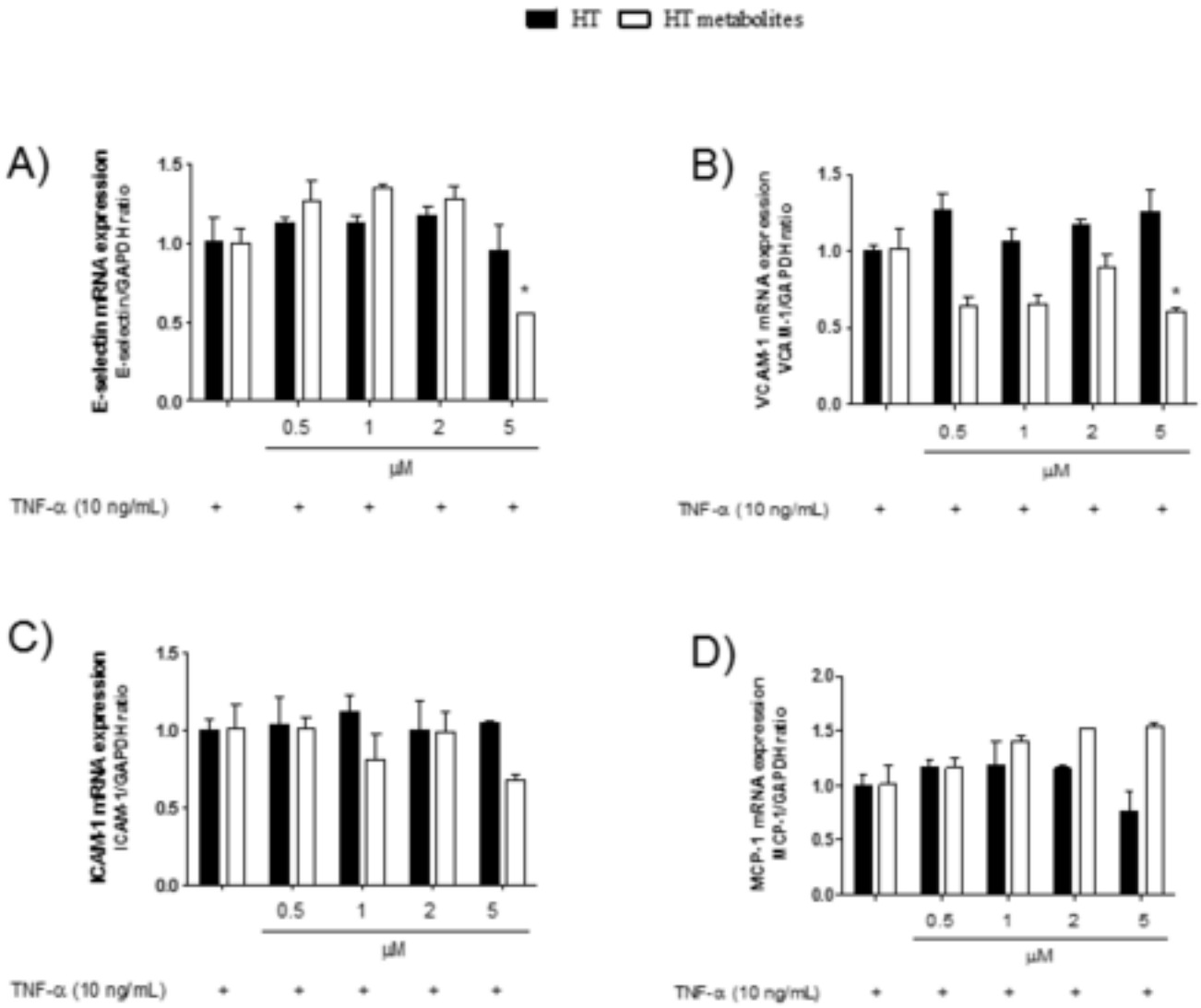

Figure 4

Click here to download high resolution image

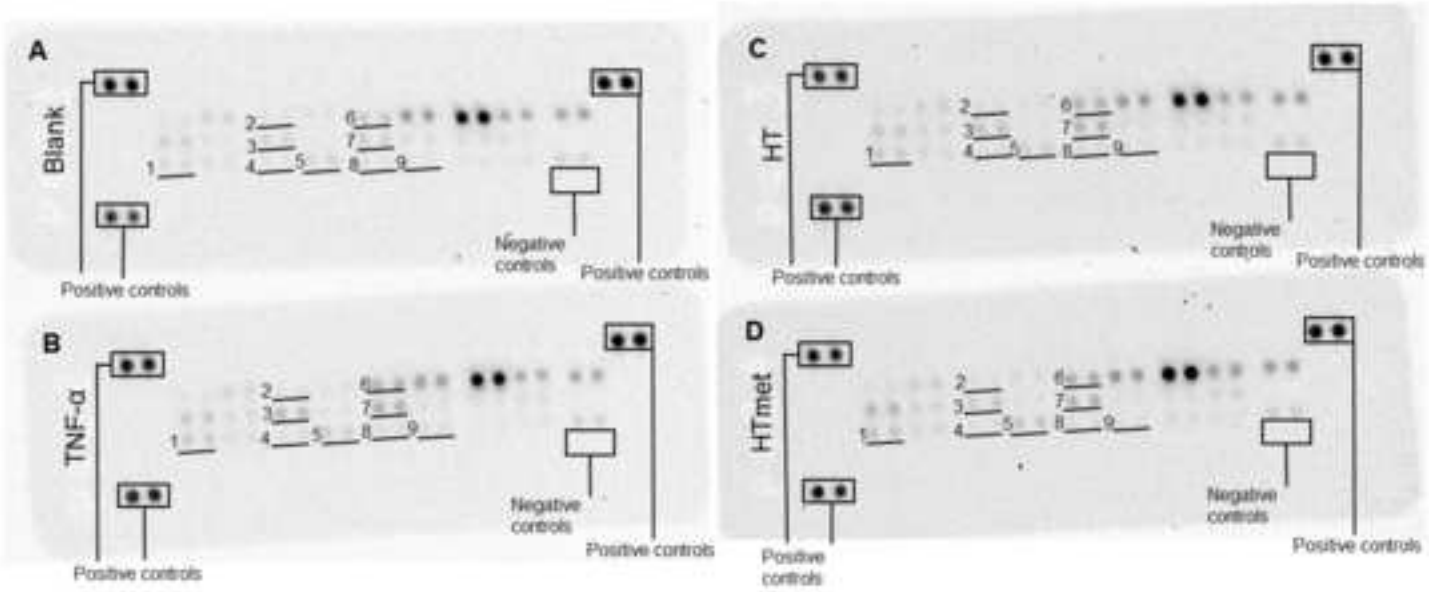

1. p38α
2. Akt3
3. JNK2
4. p38δ
5. p38γ
6. CREB
7. JNK pan
8. p53
9. P70 S6 Kinase

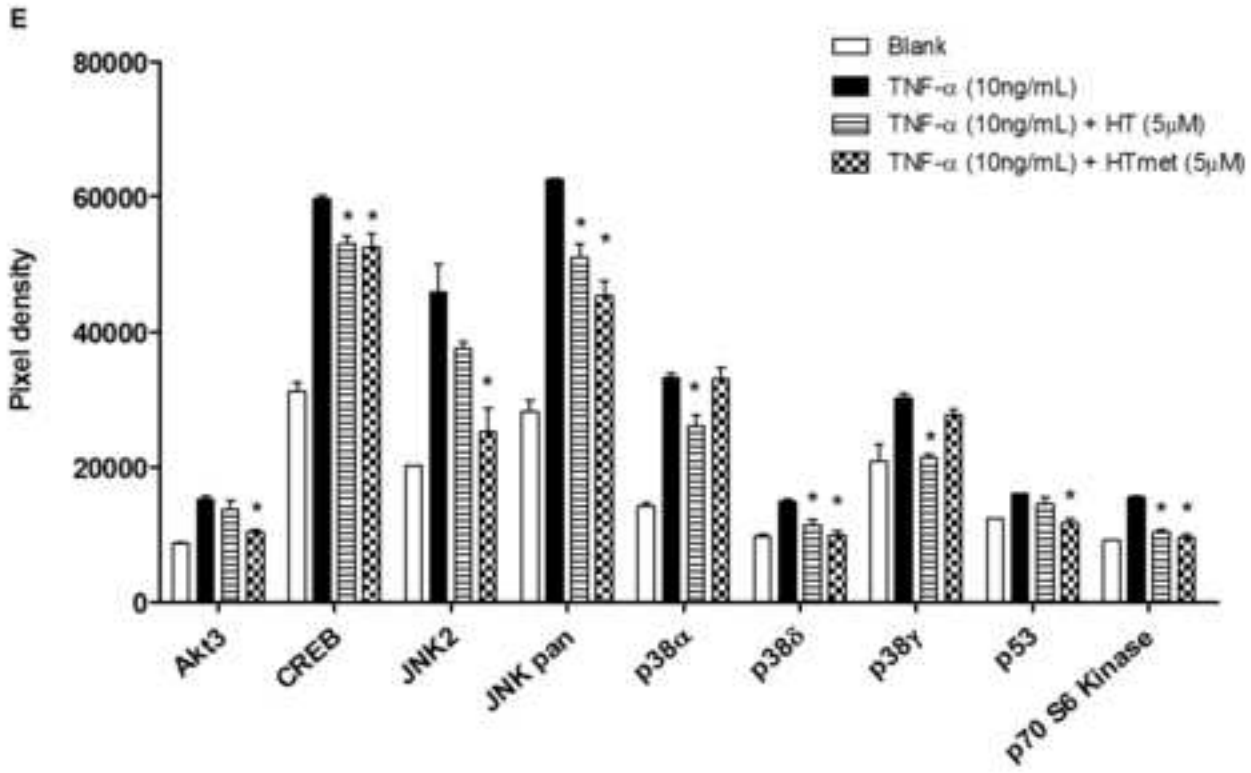

Figure 5

Click here to download high resolution image

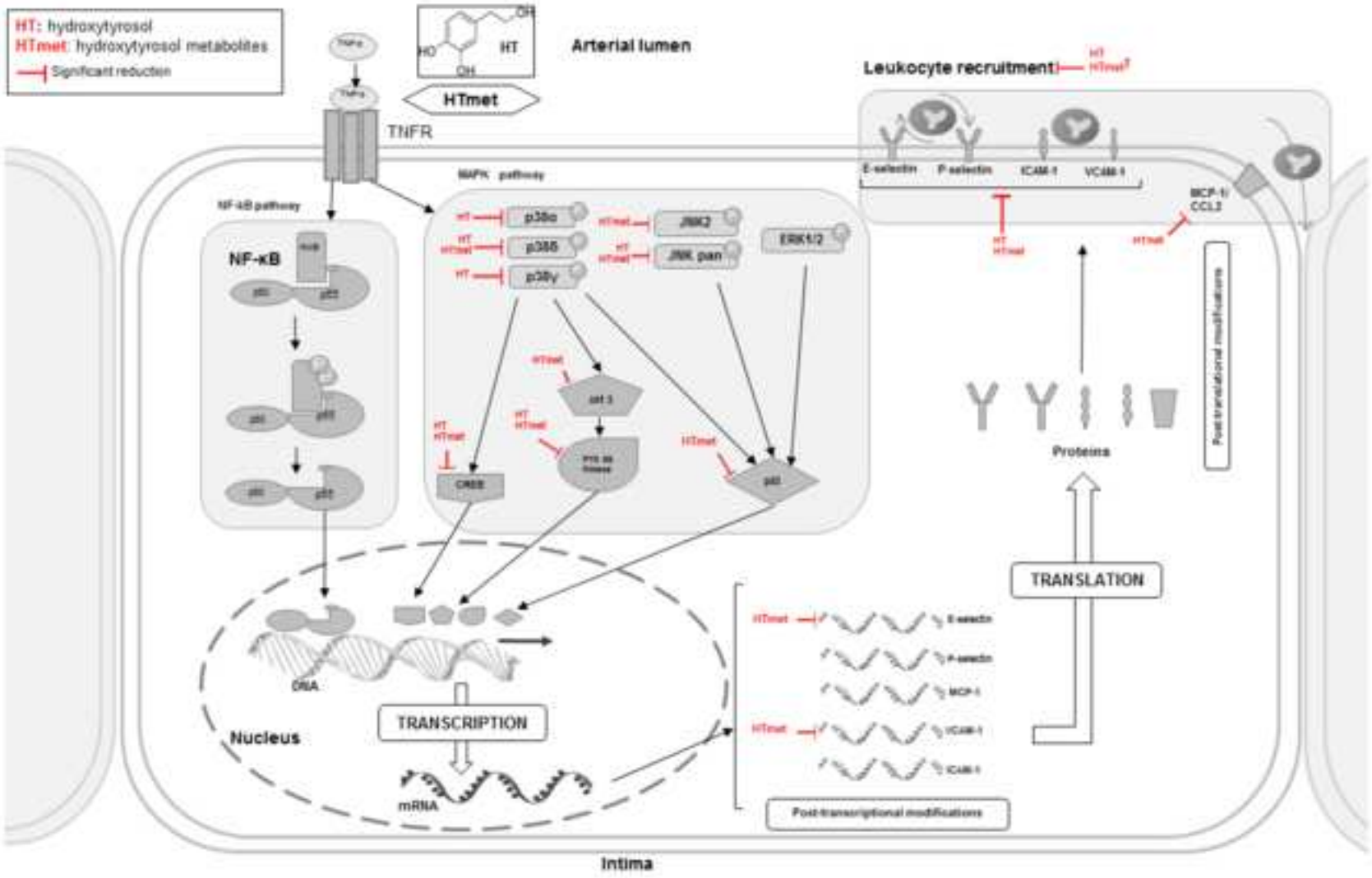

Supplemental figure 1

Click here to download high resolution image

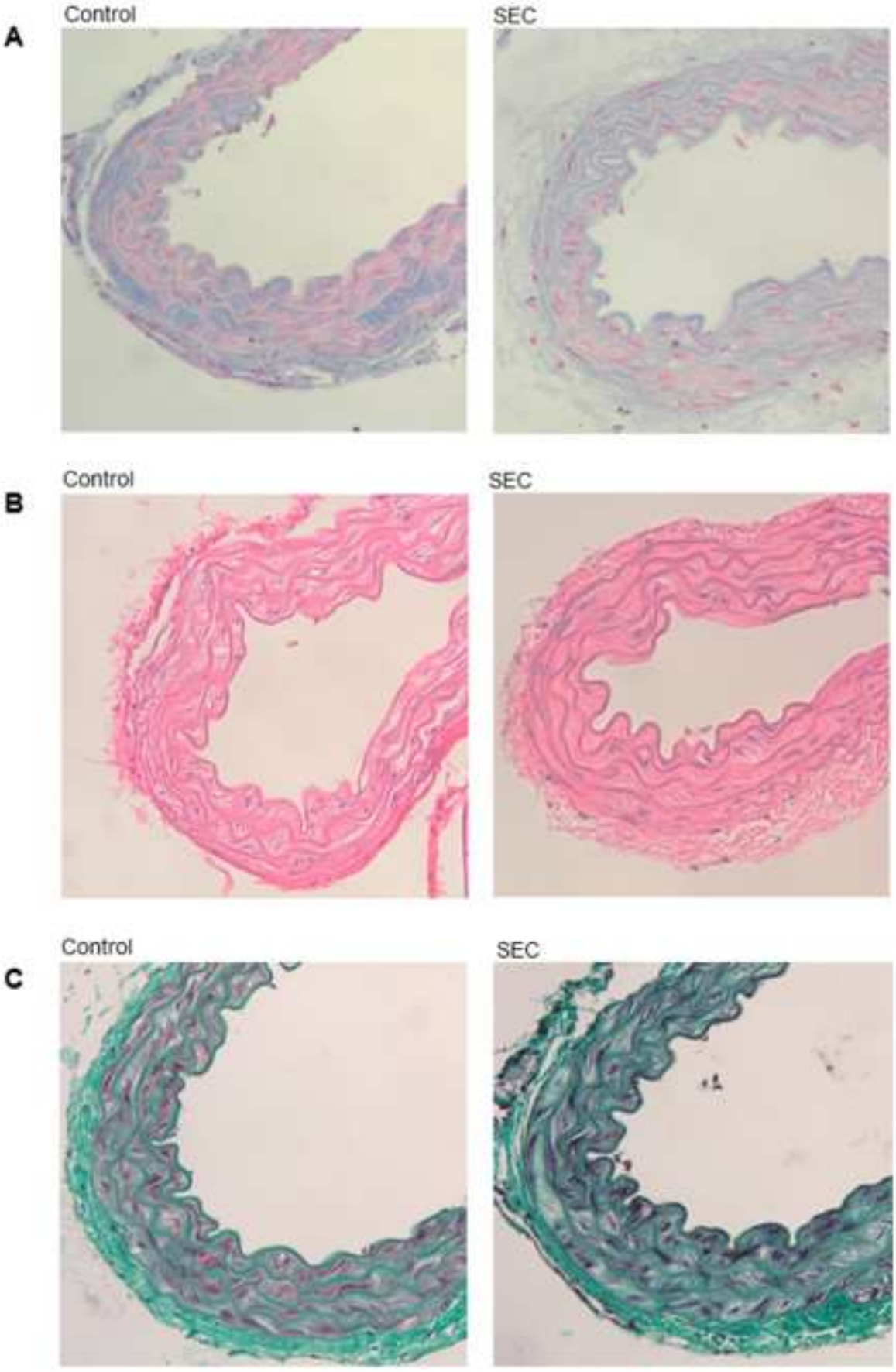

Supplemental figure 2

Click here to download high resolution image

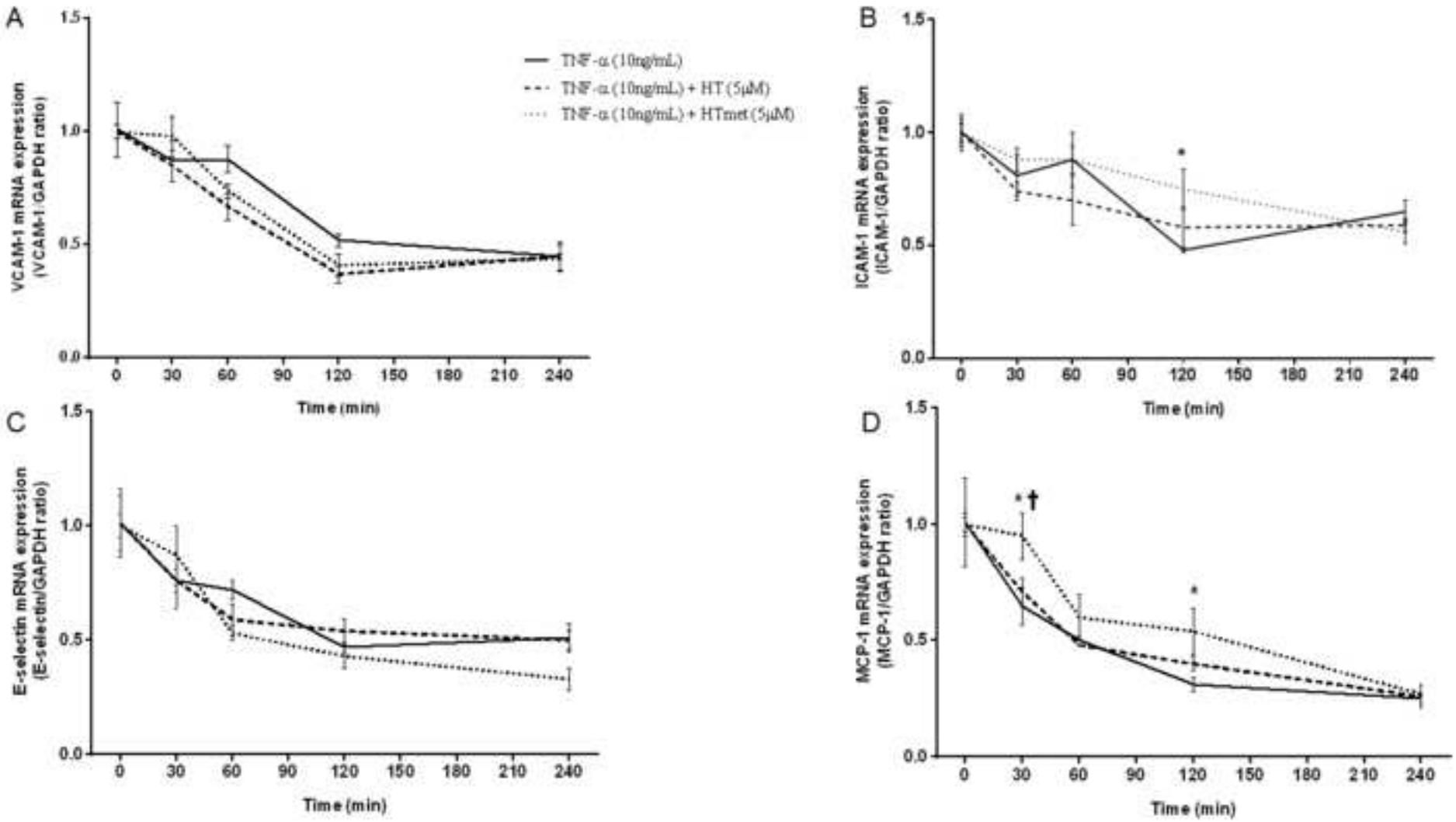

Supplemental figure 3

Click here to download high resolution image